Downloaded from genome.cshlp.org on June 25, 2026 . Published by Cold Spring Harbor Laboratory Press

Polycomb misregulation in enterocytes drives tissue decline in the aging *Drosophila* intestine

Sarah Leichter, Kami Ahmad and Steve Henikoff

Genome Res. published online November 17, 2025
Access the most recent version at doi:10.1101/gr.281058.125

P<P Published online November 17, 2025 in advance of the print journal.

Accepted Manuscript Peer-reviewed and accepted for publication but not copyedited or typeset; accepted manuscript is likely to differ from the final, published version.

Open Access Freely available online through the *Genome Research* Open Access option.

Creative Commons License This manuscript is Open Access.This article, published in *Genome Research*, is available under a Creative Commons License (Attribution 4.0 International license), as described at http://creativecommons.org/licenses/by/4.0/.

Email Alerting Service Receive free email alerts when new articles cite this article - sign up in the box at the top right corner of the article or **click here.**

To subscribe to *Genome Research* go to:
https://genome.cshlp.org/subscriptions

Published by Cold Spring Harbor Laboratory Press

Downloaded from genome.cshlp.org on June 25, 2026 . Published by Cold Spring Harbor Laboratory Press

1 # **Polycomb misregulation in enterocytes drives tissue decline in the aging**
2 ***Drosophila* intestine**

3 Sarah M. Leichter[1], Kami Ahmad[1], Steven Henikoff[1,2]*

4 **Affiliations:**

5 [1]Basic Sciences Division, Fred Hutchinson Cancer Center, Seattle, WA, USA

6 [2]Howard Hughes Medical Institute, Chevy Chase, MD, USA

7 *Corresponding author: Email: steveh@fredhutch.org

8

9 Running title: Single-cell H3K27me3 of the aging *Drosophila* gut

10

Downloaded from genome.cshlp.org on June 25, 2026 . Published by Cold Spring Harbor Laboratory Press

11 **Abstract**
12
13 Aging compromises intestinal integrity, yet the chromatin changes driving this decline
14 remain unclear. Polycomb-mediated repression is essential for silencing developmental
15 genes, but this regulatory mechanism becomes dysregulated with age. Although shifts in
16 Polycomb regulation within intestinal stem cells have been linked to gut aging, the
17 Polycomb landscape of differentiated cell types remains unexplored. Differentiated cells
18 comprise the majority of the gut epithelium and directly impact both tissue and whole
19 organismal aging. Using single-cell chromatin profiling of the *Drosophila* intestine, we
20 identify cell-type-specific chromatin landscape changes during aging. We find that old
21 enterocytes aberrantly repress genes essential for transmembrane transport and chitin
22 metabolism, contributing to intestinal barrier decline – an example of antagonistic
23 pleiotropy in a regenerative tissue. Barrier decline leads to derepression of JAK/STAT
24 ligands in all cell types and increased proliferation of aging stem cells, with elevated RNA
25 Polymerase II (RNAPII) at S-phase-dependent histone genes. Specific upregulation of
26 histone genes during aging stem cell proliferation resembles RNAPII hypertranscription
27 of histone genes in aggressive human cancers. Our work reveals that misregulation of
28 the Polycomb-mediated H3K27me3 histone modification in differentiated cells during
29 aging not only underlies tissue decline but also mirrors transcriptional changes in cancer,
30 suggesting a common mechanism linking aging and cancer progression.
31
32 **Key words:** intestinal stem cells; Polycomb domains; sciCUT&Tag; chitin synthase;
33 chitinase; Metchnikoff

34 **Introduction**

Downloaded from genome.cshlp.org on June 25, 2026 . Published by Cold Spring Harbor Laboratory Press

35 Aging is associated with the decline of tissue function and is the leading risk factor in a
36 multitude of diseases (Niccoli and Partridge 2012). The chromatin landscape of cells
37 undergoes profound changes during aging, including redistribution of Polycomb-mediated
38 repressive marks such as tri-methylation of histone H3 at lysine 27 (H3K27me3)
39 (Emerson and Lee 2023). For example, global gains in H3K27me3 and widespread
40 heterochromatinization have been observed in the livers of aged mice (Yang et al. 2023)
41 and in the muscles of aging *Drosophila* (Ma et al. 2018) leading to transcriptional
42 silencing. Forcing aged mouse liver cells to re-enter the cell cycle partially restores a
43 youthful H3K27me3 landscape, suggesting that DNA replication may rejuvenate
44 chromatin structure (Yang et al. 2023). However, even mitotically active somatic stem
45 cells display age-related increases in Polycomb repression: aged *Drosophila* intestinal
46 stem cells and mouse hematopoietic stem cells exhibit elevated dimethylation of the H3-
47 K27 residue (H3K27me2) and H3K27me3 levels, respectively, and partial differentiation
48 linked to these changes (Sun et al. 2014; Tauc et al. 2021).
49 These observations suggest that changes in Polycomb-mediated repression contribute
50 to age-associated functional decline. Supporting this, heterozygous loss-of-function
51 mutations in Polycomb group proteins such as the histone methyltransferase *Enhancer*
52 *of zeste* (*E(z)*) lead to lifespan extension (Siebold et al. 2010), implying that Polycomb
53 repression is detrimental in older animals. Yet, Polycomb group proteins are essential for
54 development (Boyer et al. 2006; Blackledge and Klose 2021) and homozygous mutants
55 are lethal (Denell and Frederick 1983) suggesting that while Polycomb activity is
56 beneficial during development, it may become detrimental with age.

Downloaded from genome.cshlp.org on June 25, 2026 . Published by Cold Spring Harbor Laboratory Press

57 Whereas Polycomb-mediated repression appears to underlie age-associated tissue
58 dysfunction, investigations have so far been limited to post-mitotic or stem cell systems,
59 overlooking regenerative tissues made up of both stem and differentiated cells. The adult
60 *Drosophila* intestine offers a model for regenerative tissues because the epithelium
61 undergoes continuous cell turnover, with a median cellular lifespan for differentiated cells
62 of four days (Liang et al. 2017). This rapid turnover ensures that both young and aged
63 intestines maintain similar cellular age distributions. Despite this, the *Drosophila* intestine
64 displays a distinctive age-related decline. Key features include barrier dysfunction, which
65 promotes microbial dysbiosis and systemic inflammation (Rera et al. 2011; Rera et al.
66 2012; Martins et al. 2018; Salazar et al. 2023), as well as an increase in stem cells (Biteau
67 et al. 2008; Rodriguez-Fernandez et al. 2020; Tauc et al. 2021). Tauc et al. demonstrated
68 that aged intestinal stem cells mis-express lineage-specific markers via altered
69 accessibility at Polycomb-regulated loci. However, differentiated cells comprise a majority
70 of the epithelium (Micchelli and Perrimon 2006; Ohlstein and Spradling 2006) and defects
71 in these cells alone have been shown to cause systemic aging (El Mai et al. 2023). Given
72 the rapid turnover of differentiated cells, age-dependent changes in Polycomb-mediated
73 silencing in differentiated cells could be a major driver of tissue dysfunction.

74 In this study we aim to test this hypothesis through single-cell profiling of the H3K27me3
75 mark in the *Drosophila* intestine to distinguish cell types and capture cell-type-specific
76 dynamics of Polycomb-associated modifications during aging.

77 **Results**

78 **Single-cell chromatin profiling of the fly gut**

Downloaded from genome.cshlp.org on June 25, 2026 . Published by Cold Spring Harbor Laboratory Press

79 The epithelium of the *Drosophila* adult gut is composed of four cell types: intestinal stem
80 cells, enteroblasts, enterocytes, and enteroendocrine cells (Micchelli and Perrimon 2006;
81 Ohlstein and Spradling 2006). Intestinal stem cells divide symmetrically to populate the
82 niche or asymmetrically to birth an enteroblast, an undifferentiated progenitor cell that
83 differentiates into an enterocyte or enteroendocrine cell (Micchelli and Perrimon 2006;
84 Ohlstein and Spradling 2006). Enterocytes are the most abundant cell type in the
85 *Drosophila* gut and primarily function in absorption and transportation of nutrients and
86 secretion of digestive enzymes, while enteroendocrine cells secrete gut hormones (Hung
87 et al. 2020). Immunostaining of guts from 1-day-old *esg-GAL4, UAS-GFP* female flies,
88 which marks intestinal stem cells/enteroblasts (ISC/EBs) with high level of GFP
89 expression, displays distinct cell sizes and levels of GFP expression (Fig. 1A). ISC/EB
90 cell nuclei are small with strong GFP expression, while enteroendocrine nuclei are also
91 small with low level of GFP expression. Finally, enterocytes have large polyploid nuclei
92 with no GFP expression. Additionally, each cell type displays distinct patterns of
93 H3K27me3 staining, implying that gut cell types may be distinguished by chromatin
94 landscapes of this histone modification. We used single-cell combinatorial indexing
95 CUT&Tag (sciCUT&Tag) to barcode cells in a profiling experiment (Janssens et al. 2024).
96 Anticipating that we would compare single cells from different ages, we dissociated guts
97 from female flies of different ages in replicate in one experiment. We chose three ages to
98 span adulthood in *Drosophila*: 1 day after eclosion (young), 15 days after eclosion
99 (middle-aged), and 40 days after eclosion (old aged). Forty guts from virgin females of
100 each age were barcoded by tagmentation, and then cells were arrayed on two ICELL8
101 chips for barcoded PCR (Supplemental Table S1). Peaks were called on the aggregate

Downloaded from genome.cshlp.org on June 25, 2026 . Published by Cold Spring Harbor Laboratory Press

102 data for each age using SEACR (Meers et al. 2019), then merged for dimensionality
103 reduction and uniform manifold approximation and projection (UMAP) embedding in
104 ArchR (Granja et al. 2021) (Supplemental Table S2). We applied multiple filtering steps
105 to retain cells that had fragment counts of at least 100 (Supplemental Table S3), a high
106 fraction of reads in peaks (FRiP, Supplemental Table S4) and a low fraction of blacklisted
107 reads (Amemiya et al. 2019) (Supplemental Table S5), which after removing doublets
108 yielded 40,982 cells for analysis.

109 To assign cell types using a repressive modification, we calculated chromatin silencing
110 scores (CSS) (Wu et al. 2021), where low CSS indicates that a gene is not repressed and
111 could be expressed, and high scores indicate a gene is repressed. Chromatin silencing
112 scores anti-correlate with cell-type-specific gene expression profiles (Wu et al. 2021).
113 Using ArchR for clustering and then scoring known marker genes for each cell type (Hung
114 et al. 2020), we identified individual cells as ISC/EBs with low CSS at the escargot (*esg*)
115 gene, enteroendocrine cells at the Piezo gene, and enterocytes at the nubbin (*nub*) gene
116 (Supplemental Fig. S1A). We were unable to separate intestinal stem cell from
117 enteroblasts so we group them together as an ISC/EB cluster for subsequent analyses.
118 These three cell types form five distinct clusters on the gut UMAP; one of ISC/EBs, one
119 of enteroendocrine cells, and three clusters of enterocytes (Fig. 1B).

120 First focusing on young guts, our analysis includes 11,586 young cells with 68% (7,913)
121 of the cells called as enterocytes (Supplemental Table S6). Enterocytes have the highest
122 fragments per cell (Fig. 1C), which might be due to more widespread repression in this
123 cell type, and/or to polyploidy of these cells. To identify the genes repressed between cell
124 types, we performed differential analysis for genes that fall within H3K27me3-marked

Downloaded from genome.cshlp.org on June 25, 2026 . Published by Cold Spring Harbor Laboratory Press

125 domains as determined using our SEACR peaks (Supplemental Tables S7-S10).
126 H3K27me3-marked domains stretch multiple kilobases in length such as the canonical
127 Antennapedia-Complex (*ANTP-C*), bithorax-complex (*BX-C*), and the Posterior sex
128 combs-Suppressor of zeste 2 (*Psc-Su(z)2*) domains (Schwartz et al. 2006), which are
129 shared across the three cell types (Fig. 1E and Supplemental Fig. S1B, C). There are
130 regions that fall outside of the canonical domains, such as at the rotund (*rn*) gene, that
131 appear to be H3K27me3-marked in enteroendocrine and ISC/EBs, but not enterocytes
132 (Fig. 1E), indicating differences in the H3K27me3 landscape between the cell types. Of
133 the 8,697 genes in domains, 10.7% (933) show differential signal between the young cell
134 types from differential analysis (Fig. 1D and Supplemental Table S11). Genes in cell-type
135 specific domains include the *42AB* piRNA cluster (Fig. 1F), which is positively regulated
136 by the H3K27me3 modification in *Drosophila* ovarian stem cells (Akkouche et al. 2025),
137 but is expressed at low levels in the gut (Siudeja et al. 2021). In differentiated cells, the
138 non-coding RNA lncRNA:CR32773 forms an H3K27me3 domain in enteroendocrine cells
139 (Fig. 1G) and held out wings (*how*) is H3K27me3-marked in enterocytes (Fig. 1H). Some
140 genes are marked with the H3K27me3 modification in two cell types but not the third:
141 enterocytes and enteroendocrine cells share a greater number of common H3K27me3-
142 marked genes with ISC/EBs (122 genes, cluster 6 and 191 genes, cluster 5, respectively)
143 than they do with each other (51 genes, cluster 1) (Fig. 1D). We interpret this pattern as
144 evidence of lineage-specification, where differentiated cells retain H3K27me3 marks from
145 their cell of origin (ISC/EBs) and therefore resemble progenitors more closely than they
146 resemble each other. We conclude that sciCUT&Tag effectively separates the cell types
147 of the gut and identifies repressed domains characteristic of each cell type.

Downloaded from genome.cshlp.org on June 25, 2026 . Published by Cold Spring Harbor Laboratory Press

148 **Gains and losses of repression in aging cells**

149 Next, coloring the gut H3K27me3 single-cell UMAP (Fig. 1B) based on the three ages of
150 each cell type reveals that ISC/EBs of different ages are intermixed, as are
151 enteroendocrine cells (Fig. 2A, B). This indicates relatively small changes to the
152 chromatin landscapes of these two cell types as animals age. Enterocytes from each age
153 form distinct clusters (Fig. 2C), implying that the chromatin landscape of this cell type
154 changes drastically with age. We also compared fragment counts per cell across ages
155 and lineages, which showed a modest but significant increase with age (Supplemental
156 Fig. S2).

157 To map age-dependent changes in H3K27me3 landscapes for each cell type, we
158 performed differential analysis between young and old clusters (Supplemental Table S12-
159 S14). We identified 75 genes where H3K27me3 changes in ISC/EBs (Fig. 2D), 277 genes
160 in enteroendocrine cells (Fig. 2E), and 1588 genes in enterocytes (Fig. 2F). Among the
161 genes that lose H3K27me3 signal in both ISC/EBs and enteroendocrine cells, GO
162 analysis revealed enrichment for transcriptional regulators and RNA Polymerase II
163 (RNAPII) associated functions (Supplemental Fig. S3A ,B, Supplemental Tables S15,
164 S16). This included derepression of multiple transcription factor genes such as worniu
165 (*wor*) in ISC/EBs and Ets at 21C (*Ets21C*) in enteroendocrine cells, which are involved in
166 stem cell proliferation and fate decisions (Supplemental Fig. S3C, D).

167 In enterocytes, we observed both gains and losses of H3K27me3 with age, where 710
168 genes decreased in H3K27me3 signal while 878 increased in H3K27me3 signal. The
169 genes that decreased in H3K27me3 signal with age are strong domains in young cells.
170 For example, a domain encompassing the pointed (*pnt*) and oo18 RNA-binding protein

Downloaded from genome.cshlp.org on June 25, 2026 . Published by Cold Spring Harbor Laboratory Press

171 (*orb*) genes loses the H3K27me3 mark (Fig. 2G). By contrast, genes that gained
172 H3K27me3 signal with age are weak domains in young cells. An example of this is the
173 Multi drug resistance 50 (*Mdr50*) gene (Fig. 2H), which encodes an efflux transmembrane
174 transporter expressed in the midgut involved with xenobiotic transport activity and
175 response to insecticide (Denecke et al. 2017). These findings suggest that aging not only
176 weakens pre-existing Polycomb domains but also establishes new repressive marks in
177 differentiated intestinal cells, reshaping the chromatin landscape in a cell-type-specific
178 manner.

179 **Changes in repression at regulatory elements with age**

180 A major advantage of sciCUT&Tag is the ability to directly profile changes at regulatory
181 elements, which single-cell RNA sequencing (scRNA-seq) does not capture. To identify
182 regulatory elements that exhibit changes in H3K27me3 level with age within each cell
183 type, we identified self-transcribing active regulatory region sequencing (STARR-seq)
184 enhancers (Zabidi et al. 2015) that fell within our list of H3K27me3 peaks, acknowledging
185 that this list may miss gut-specific sites. From differential analysis, we identified 18
186 enhancers that changed with age in ISC/EBs and 406 in enterocytes, but none in
187 enteroendocrine cells (Supplemental Fig. S4A, B; Supplemental Tables S17, S18).

188 Next, we searched for transcription factor motifs within enhancers that significantly
189 change within each cell type using FIMO (Grant et al. 2011) against the JASPAR insect
190 transcription factor database (Rauluseviciute et al. 2024). We find in aged ISC/EBs,
191 enhancers that lose H3K27me3 are enriched for motifs linked to chromatin organization
192 and developmental regulation (e.g., Chromatin-linked adaptor for MSL proteins (CLAMP),
193 snail (sna), buttonhead (btd), and Kr transcription factor (Kr)) (Supplemental Fig. S4C).

Downloaded from genome.cshlp.org on June 25, 2026 . Published by Cold Spring Harbor Laboratory Press

194 In contrast, those that gain H3K27me3 signal show motifs for developmental regulators
195 such as twist (twi), hb transcription factor (hb), and tinman (tin) (Supplemental Fig. S4D).
196 In enterocytes, motifs for stress-responsive TFs and motifs for Trithorax-like (Trl) and
197 grainy head (grh), which are known to influence enhancer accessibility, dominate in
198 enhancers losing H3K27me3 signal (Supplemental Fig. S4E). At the same time,
199 architectural proteins such as CTCF and Motif 1 Binding Protein (M1BP) are enriched in
200 enhancers that gain H3K27me3 signal with age (Supplemental Fig. S4F). Notably,
201 CLAMP motifs appear consistently across cell types, enriched in enhancers that both lose
202 and gain H3K27me3 signal with age. CLAMP has been shown to displace Trl/GAF during
203 stress and act as a transcriptional repressor (Aguilera et al. 2025). Together, these
204 findings suggest that CLAMP functions in a context-dependent manner during aging,
205 contributing to both repression and derepression of enhancer activity under stress-
206 associated conditions. These results point to chromatin-level changes that may prime
207 these cells for altered transcriptional programs with age.

208 **Polycomb repression of barrier membrane genes in aging enterocytes**

209 A major defect of the aging *Drosophila* gut is breakdown of the protective barrier
210 membrane (Salazar et al. 2023). This is observed through the 'Smurf Assay' in which flies
211 are fed food containing a non-absorbable blue dye that stains only the digestive tract of
212 young flies where the intestinal barrier is intact, but in old flies the blue dye spreads
213 through the whole body due to increased permeability of the gut (Rera et al. 2011; Rera
214 et al. 2012; Martins et al. 2018) (Fig. 3A). Given that elevated H3K27me3 levels have
215 been associated with reduced lifespan (Siebold et al. 2010; Ma et al. 2018), we

Downloaded from genome.cshlp.org on June 25, 2026 . Published by Cold Spring Harbor Laboratory Press

216 hypothesized that age-related changes in the H3K27me3 landscape of enterocytes may
217 contribute to barrier dysfunction.

218 To investigate this, we performed GO analysis of genes that gain or lose H3K27me3
219 signal in aged enterocytes (Supplemental Tables S19, S20). Among the genes that lose
220 H3K27me3 signal with age, top GO terms include “neurogenesis”, “regulation of
221 transcription by RNA Polymerase II”, “generation of neurons”, and “transcription by RNA
222 Polymerase II” (Supplemental Fig. S5A), which resulted in a list of transcription factor
223 genes involved in development and differentiation that become derepressed with age
224 (Supplemental Fig. S5B). Notably, this group includes the Enhancer of Split (*E(spl)*)
225 complex genes, located on Chromosome *3R*, which are normally Polycomb-repressed in
226 young enterocytes (Josserand et al. 2023) (Supplemental Fig. S5C) as well as the HOX
227 transcription factor paired (*prd*) (Supplemental Fig. S5D). These findings mirror the
228 chromatin derepression of transcription factor genes in aged ISC/EBs and
229 enteroendocrine cells, consistent with a widespread relaxation of lineage-specific
230 repression programs during aging.

231 In contrast, GO analysis of genes that gain H3K27me3 signal in aged enterocytes reveal
232 enrichment for the terms “transmembrane transport”, “tissue morphogenesis”,
233 “morphogenesis of an epithelium”, and “aminoglycan metabolic process” (Fig. 3B). Of
234 particular interest is this last term, as the barrier that forms over the intestinal epithelium
235 protecting it from contents from the lumen, the peritrophic matrix, is composed of the
236 aminoglycan chitin (Lehane 1997). The peritrophic matrix of insects is analogous to the
237 mammalian mucus-based membrane of the digestive track (Konno and Mitsuhashi 2019),
238 is produced in the foregut, and midgut enterocytes produce chitin to maintain the

Downloaded from genome.cshlp.org on June 25, 2026 . Published by Cold Spring Harbor Laboratory Press

239 peritrophic matrix (Dutta et al. 2015; Zhu et al. 2024). Disruption of chitin secretion from
240 enterocytes to the peritrophic matrix leads to barrier dysfunction and susceptibility to
241 stress (Katheder et al. 2023). Two gut-specific genes that acquire strong H3K27me3-
242 marked domains in aged enterocytes are Chitin synthase 2 (*Chs2*) and Chitinase 9 (*Cht9*)
243 (Fig. 3C, D). Both of these genes are involved in maintenance of the peritrophic matrix
244 and in the midgut are expressed in enterocytes (Supplemental Table S21) (Buchon et al.
245 2013; Hung et al. 2020). Degradation of chitin and silencing of *Chs2* are key targets for
246 the development of insecticides against pests such as mosquitos (Zhang et al. 2023).
247 *Cht9* is specifically expressed in the gut (Leader et al. 2018; Krause et al. 2022) but is
248 clustered together with three other chitinases (Chitanse *8* (*Cht8*), Chitinase 12 (*Cht12*),
249 and Chitinase 4 (*Cht4*)) that all become marked with H3K27me3 with age (Fig. 3D). The
250 H3K27me3 domains only form over *Chs2* and the *Cht4-8-9-12* chitinase gene clusters in
251 aged enterocytes, implying that they become repressed in older animals (Supplemental
252 Fig. S6A, B).

253 To determine if the increase in H3K27me3 signal across the domain leads to
254 transcriptional silencing of *Chs2* and *Cht9*, we profiled the initiating serine-5
255 phosphorylated isoform of RNA Polymerase II (RNAPIIS5P) in whole guts using
256 CUT&Tag under CUTAC low-salt tagmentation conditions (Henikoff et al. 2020; Janssens
257 et al. 2022) (Supplemental Tables S1, S22). RNAPIIS5P provides a direct view of ongoing
258 transcriptional engagement and promoter-proximal regulation that RNA-seq does not
259 capture.

260 Previously published single-cell RNA-seq data from the aging Drosophila intestine (Tauc
261 et al. 2021) were generated from FACS-isolated cells, resulting in datasets heavily

Downloaded from genome.cshlp.org on June 25, 2026 . Published by Cold Spring Harbor Laboratory Press

262 enriched for ISCs and EBs, with few differentiated cells represented (Supplemental Table
263 S23). In contrast, our single-cell H3K27me3 and bulk RNAPII-S5P datasets were
264 generated from whole guts without cell sorting. Because of these fundamental differences
265 in sample composition and experimental design, the published single-cell RNA-seq data
266 are not directly compatible for integration with our H3K27me3 sciCUT&Tag dataset.

267 We performed four replicates of RNAPIIS5P CUTAC per age and identified a high
268 Pearson's correlation between replicates within an age group, allowing us to merge the
269 four replicates for analysis (Supplemental Fig. S7). We found that RNAPIIS5P is present
270 at the promoters of the *Chs2, Cht4 and Cht9* genes in young tissues and lacking at *Cht12*,
271 which is not expressed in this tissue (Leader et al. 2018; Krause et al. 2022). For the three
272 genes that are expressed, signal decreases with age (Fig. 3E, Supplemental Fig. S8A, B,
273 confirming that these genes become repressed. From differential analysis between young
274 and old guts, *Chs2* and *Cht9* are significantly repressed with age (Supplemental Table
275 S24).

276 We next asked why H3K27me3 would accumulate over chitin genes with age. The
277 H3K27me3 mark is bound by the Polycomb chromodomain protein (Pc) (Cao et al. 2002),
278 but Pc is also localized at the promoters of many active genes (Orsi et al. 2014). Given
279 the duality of Pc binding, we profiled the Pc protein in all three ages of whole guts by
280 CUT&Tag (Supplemental Tables S1, S25). We found that Pc binds promoters both within
281 and outside of H3K27me3-marked domains identified across all three cell types and ages.
282 In the intestine, a larger fraction of promoters fall within H3K27me3-marked domains
283 because cells of this tissue exhibit more broadly repressed chromatin than previously
284 profiled Drosophila tissues (Supplemental Fig. S9A, B). Genome-wide analyses have

Downloaded from genome.cshlp.org on June 25, 2026 . Published by Cold Spring Harbor Laboratory Press

285 shown that the majority of Pc binding sites in other Drosophila tissues are located outside
286 of H3K27me3-marked domains (Orsi et al. 2014; Loubiere et al. 2016; Brown et al. 2018).
287 Promoter-proximal Pc sites outside of H3K27me3 domains differ from Pc occupancy
288 within domains, where Pc is predominantly anchored at Polycomb Response Elements
289 (PREs).

290 We observe minimal changes in Pc signal across ages (Supplemental Fig. S9A, B). For
291 example, the H3K27me3 domain around the gene senseless-2 (*sens-2*) is present in all
292 three cell types and contains multiple Pc binding sites that are stable with age
293 (Supplemental Fig. S9C). In contrast, Sphingosine-1-phosphate lyase (*Sply*) lacks the
294 H3K27me3 mark and is therefore not located within a domain but is bound by Pc
295 (Supplemental Fig. S9D), consistent with prior reports that Pc can localize independently
296 of H3K27me3 (Schaaf et al. 2013; Orsi et al. 2014; Loubiere et al. 2016).

297 When we examined Pc level at the promoters of chitin genes we found that it is present
298 around the active promoters of the *Chs2* and *Cht9* genes in young guts (Fig. 3F, G) and
299 in older tissues (Fig. 3H, Supplemental Fig. S7C, D), with high specificity compared to the
300 promoters of genes lacking Pc signal, such as the promoters of the genes radish (*rad*)
301 and dusky (*dy*) (Supplmental Fig. S8E, F). Although the signal at *Cht9* appears low, it is
302 exhibits a level of signal greater than IgG, which is a non-specific antibody that serves as
303 a control for CUT&Tag (Kaya-Okur et al. 2019; Kaya-Okur et al. 2020) (Supplemental
304 Table S26). In a coverage heatmap ordered by Pc descending signal, we find *Chs2* and
305 *Cht9* to be present in the top 25% of promoters within H3K27me3 domains (Supplemental
306 Figure S8A). Thus, while the presence of Pc at these promoters is compatible with gene
307 expression in young tissues, in aged guts binding of the Pc chromodomain to H3K27me3

Downloaded from genome.cshlp.org on June 25, 2026 . Published by Cold Spring Harbor Laboratory Press

308 leads to chromatin compaction and gene repression (Kassis et al. 2017). Note, we find
309 that many Pc binding sites do not trigger the formation of a H3K27me3 domain with age
310 (Supplemental Figure S9B, D). Therefore, we hypothesize that using Pc for gene
311 regulation early in life comes with the risk of nucleating repression later in life.

312 **Derepression of enteroendocrine genes in aged guts**

313 Having established that age-dependent H3K27me3 gain in enterocytes drives barrier
314 failure, we next asked how Polycomb changes in the aged ISC/EB lineage. Previous
315 studies have reported an age-related increase in enteroendocrine precursor cells,
316 identified by co-expression of intestinal stem cell and enteroendocrine markers, which is
317 linked to changes in chromatin accessibility of Polycomb-regulated loci (Tauc et al. 2021).
318 Using the set of genes marked by H3K27me3 in young enteroendocrine cells from
319 differential analysis (Fig. 1D), we find that aged ISC/EBs gain H3K27me3 signal over
320 many enteroendocrine-marked genes (124 of 205) including Nopp140*,* warts (*wrts*)*,* and
321 Drip (Fig. 4A), indicating that aged ISC/EBs begin to acquire an H3K27me3 landscape
322 that partially resembles that of enteroendocrine cells, although these cells still cluster with
323 ISC/EBs in our UMAP (Figure 2A). We also observed the loss of signal at a subset of
324 H3K27me3-marked enteroendocrine genes in aged ISC/EBs, including transcription
325 factors such as *Ets21C* and invected *(inv*), and the slit receptor roundabout2 (*robo2*) (Fig.
326 4A). *Robo2* restricts ISC commitment to the enteroendocrine lineage through repression
327 of prospero (Biteau and Jasper 2014). The loss of H3K27me3 at *robo2* in aged progenitor
328 cells may reflect a compensatory mechanism that preserves some stem cell identity by
329 restricting full differentiation into the enteroendocrine lineage. This suggests that aged
330 ISC/EBs adopt a chromatin landscape partially resembling that of enteroendocrine cells,

Downloaded from genome.cshlp.org on June 25, 2026 . Published by Cold Spring Harbor Laboratory Press

331 consistent with the model in which aged stem cells exhibit partial differentiation toward
332 the enteroendocrine fate (Tauc et al. 2021). To further support this conclusion, we
333 examined additional genes in aged ISC/EBs that have been identified as markers of
334 enteroendocrine precursors and neural stem cell potential, including *sna*, *wor*, and
335 *deadpan* (*dpn*) (Tauc et al. 2021). These genes lose H3K27me3 signal in aged ISC/EBs
336 (Supplemental Fig. S10), reinforcing the model that aging pushes progenitor cells toward
337 partial differentiation into the enteroendocrine lineage.

338 **JAK/STAT ligands become derepressed in aged gut**

339 Over-proliferation of stem cells (Biteau et al. 2008) is reflected in the higher abundance
340 of ISC/EBs in older guts (Fig. 4B). Indeed, the proportion of stem cells based on single-
341 cell profiling increases from 22.4% in young tissues to 52.5% in aged tissues (Fig. 4C).
342 Stem cell over-proliferation is stimulated by production of Unpaired ligands which activate
343 the JAK/STAT pathway (Jiang et al. 2009). We observe that this domain loses the
344 H3K27me3 mark in all three cell types (Fig. 4D, Supplemental Fig. S11A). This loss is
345 accompanied by an increase in RNAPIIS5P signal at the unpaired 3 (*upd3*) promoter,
346 which is statistically significant by differential analysis (Fig. 4E, Supplemental Fig. S11B,
347 Supplemental Table S24), the unpaired gene specifically expressed in the gut (Jiang et
348 al. 2009). The unpaired 2 (*upd2*) promoter also shows increased RNAPII-S5P with age
349 (Fig. 4E, Supplemental Fig. S11C). By contrast, the unpaired 1 (*upd1*) promoter maintains
350 very low RNAPII-S5P at all ages, consistent with persistent H3K27me3 signal over the
351 *upd1* gene in all ages and cell types (Supplemental Fig. S11A, D). Expression of these
352 ligands is known to be regulated by Polycomb silencing, as knockdown of Polycomb
353 silencing components leads to loss of the H3K27me3 mark over a domain encompassing

Downloaded from genome.cshlp.org on June 25, 2026 . Published by Cold Spring Harbor Laboratory Press

354 the three unpaired genes, resulting in increased expression and to tumor formation
355 (Parreno et al. 2024). Additionally, we observe increased RNAPIIS5P at the promoters of
356 the JAK/STAT target genes Zinc finger homeodomain 1 (*zfh1*) and 2 (*zfh2*) (Supplemental
357 Fig. S11E, F). These results support the idea that as the gut ages, damaged enterocytes
358 induce derepression of JAK/STAT ligands, leading to over-proliferation of stem cells and
359 hyperplasia of the tissue.

360 **S-phase-dependent histone gene upregulation with cell proliferation**

361 The increase in ISC/EB cell number prompted us to test for global gene upregulation, or
362 hypertranscription, a general feature of mammalian stem cell proliferation (Kim et al.
363 2023; Kim et al. 2024). We previously showed that hypertranscription can be detected in
364 cancer by plotting the difference in RNAPIIS5P signal between tumor and normal cells as
365 a function of the average RNAPIIS5P signal (Henikoff et al. 2025). We applied the same
366 analytical approach to *Drosophila* gut samples, for each promoter plotting the RNAPIIS5P
367 difference between each age as a function of the average signal (Altman and Bland 1983)
368 displayed on a $\log_{10}$ scale for clarity. Excluding histone genes, neither hyper- nor
369 hypotranscription was observed for the 15- to 1-day comparison (Supplemental Fig.
370 S12A), although hypotranscription was detected between 40- and 15-day-old and 40- and
371 1-day-old guts (Figure 5A, Supplemental Fig. S12B). The multiple-copy histone genes
372 were exceptional, displaying enormous enrichment of RNAPIIS5P at the multiple-copy S-
373 phase-dependent core histone genes, greater enrichment for His2A, His2B, His3 and
374 His4 than for all 21,876 other annotated promoters (Fig. 5A, Supplemental Fig. S12A, B).
375 By contrast, histone H1, the linker histone responsible for primary chromatin compaction,
376 showed lower level of enrichment with age (Figure 5B, Supplemental Fig. S12B).

Downloaded from genome.cshlp.org on June 25, 2026 . Published by Cold Spring Harbor Laboratory Press

377 Importantly, S-phase-dependent histone transcripts lack polyadenylation (Marzluff and
378 Koreski 2017) and are poorly captured by standard RNA-seq, making RNAPIIS5P
379 profiling especially suitable for assessing their transcriptional regulation. Direct
380 comparison of 40 days old versus 15 days old tissues show widespread loss of
381 RNAPIIS5P at most genes, accompanied by orders-of-magnitude higher levels at histone
382 loci (Figure 5B, C). Notably, 15 days old corresponds to the peak of gut maturation, after
383 which age-related decline begins (Capo et al. 2019). This establishes S-phase-
384 dependent histone gene upregulation as a transcriptional signature of advanced aging in
385 this tissue.

386 RNAPII accumulates at histone genes during times of rapid cell proliferation such as in
387 early *Drosophila* embryos (Huang et al. 2021) and in mouse embryonic stem cells at S-
388 phase (Mahat et al. 2024) with corresponding reductions genome-wide. As S-phase-
389 dependent histones are rate-limiting for proliferation, their specific accumulation of
390 RNAPIIS5P is consistent with histone gene transcription driving stem cell over-
391 proliferation in the gut. Whereas RNAPIIS5P increases at all four core histone genes in
392 old tissue, the genes for histone His2B and for histone His2A increase the most (Fig. 5C,
393 D), suggesting a higher demand for these histones in the aging gut. In yeast,
394 overexpression of core histone genes extends replicative lifespan, highlighting their
395 potential role in promoting cellular longevity (Feser et al. 2010). Increased RNAPIIS5P at
396 S-phase-dependent histone genes during aging-associated stem cell proliferation
397 resembles similar upregulation at orthologous histone genes in other rapidly dividing cell
398 types.

399 Discussion

Downloaded from genome.cshlp.org on June 25, 2026 . Published by Cold Spring Harbor Laboratory Press

400 Over a century ago Elie Metchnikoff hypothesized that systemic aging results from the
401 breakdown of the intestinal barrier (Metchnikoff and Mitchell 1907; Salazar et al. 2023),
402 with toxic effects inducing aging of other tissues (Rera et al. 2012). Our study provides a
403 chromatin-level mechanism for this hypothesis by showing that age-dependent gains of
404 the repressive H3K27me3 mark in enterocytes—and corresponding losses at other loci—
405 alter gene expression programs that underlie gut aging. Enterocytes accrue ectopic
406 H3K27me3 signal over multiple chitin-synthesis genes, compromising the peritrophic
407 matrix that normally shields the epithelium from luminal toxins (Zhang et al. 2023).
408 Consistent with analogous zebrafish studies showing that enterocyte-specific telomerase
409 loss drives systemic aging and that its restoration slows organismal decline (El Mai et al.
410 2023), our results underscore enterocytes as critical drivers of aging. Although previous
411 *Drosophila* studies attributed gut aging to chromatin changes in intestinal stem cells (Tauc
412 et al. 2021), our results position enterocytes as the initiating cell type: by repressing chitin-
413 related genes, aged enterocytes drive barrier failure, stem-cell hyperproliferation, and
414 likely systemic aging effects (Fig. 6). Loss of barrier integrity is not only a hallmark of gut
415 aging but also a strong predictor of imminent death (Rera et al. 2012) as toxins leaking
416 into circulation promote microbial dysbiosis, systemic inflammation, and lifespan limitation
417 (Clark et al. 2015; Li et al. 2016; Salazar et al. 2023).

418 Why would chitin synthesis genes acquire Polycomb repression in aged animals?
419 Polycomb repression is mediated by the PRC2 complex, which methylates H3K27 on
420 nucleosomes. The chromodomain of Polycomb (Pc) protein component of PRC1
421 specifically binds H3K27me3, but Pc also binds at active promoters (Schaaf et al. 2013;
422 Orsi et al. 2014). We propose that the binding of Polycomb at active promoters carries a

Downloaded from genome.cshlp.org on June 25, 2026 . Published by Cold Spring Harbor Laboratory Press

423 risk, at some low frequency, of nucleating repression. Polycomb protein occupies the
424 promoters of both the *Chs2* and *Cht9* genes in guts, and so as animals age stochastic
425 nucleation of repression would silence these critical genes, resulting in peritrophic
426 membrane breakdown and leaky guts.

427 Normal Polycomb regulation in young adult *Drosophila* but aberrant mis-regulation in
428 aged flies may be a molecular example of antagonistic pleiotropy. In this evolutionary
429 framework, genes beneficial to the organism early in life are selected for, regardless of
430 any deleterious consequences they may have later in life (Williams 1957). This framework
431 explains aging not as the inevitable breakdown of living machinery, or as a necessary
432 programmed stage of life history, but as the unselected side-effect of pleiotropic genes
433 selected for their early benefits. One such example of antagonistic pleiotropy has been
434 documented in the nematode *Caenorhabditis elegans*, where insulin signaling stimulates
435 reproduction early in life but also shortens lifespan (Jenkins et al. 2004). In this case early
436 reproduction is selected for; side-effects on lifespan are irrelevant. Antagonistic pleiotropy
437 of Polycomb regulation may also explain why genetic reduction of Polycomb components
438 extend lifespan in *Drosophila* (Siebold et al. 2010), perhaps simply by reducing silencing
439 of chitin synthesis genes in old enterocytes.

440 We also identified a small number of significant changes to the H3K27me3 landscape in
441 aged ISC/EBs, including derepression of enteroendocrine marker genes, consistent with
442 a prior report of partial differentiation of this cell type with age through Polycomb silencing
443 (Tauc et al. 2021). It is unclear if skewed lineage commitment is a cause or consequence
444 of the accumulation of defective enterocytes in aged tissues. Thus, we attribute aging in
445 the gut to the aberrant Polycomb silencing in enterocytes, which results in stimulation of

Downloaded from genome.cshlp.org on June 25, 2026 . Published by Cold Spring Harbor Laboratory Press

446 stem cells to divide, leading to increased RNAPIIS5P occupancy at the histone genes
447 (Fig. 6). While defective enterocytes may be the proximal cause of gut permeability, the
448 induction of compensatory stem cell proliferation may be responsible for other age-related
449 syndromes.

450 Notably, cancer risk is strongly associated with age (Havas et al. 2022), and reduced stem
451 cell proliferation reduces this risk (Zhuang et al. 2025). In contrast to cancer, aged guts
452 do not show hypertranscription but rather exhibit a selective increase in RNA Polymerase
453 II occupancy at histone genes, likely driven by stem cell hyper-proliferation. Other genes
454 appear to lose RNA Polymerase II occupancy. The loss at other genes may be due to
455 changes in cell type proportions with age; however, we cannot confirm this without cell-
456 type-specific RNAPIIS5P profiles. Regardless, we observe high levels of RNAPIIS5P at
457 the histone genes in old tissues, suggesting old ISC/EBs overexpress these genes. We
458 previously demonstrated that increased levels of RNA Polymerase II at histone genes
459 predicts outcome and correlates with whole-arm chromosomal losses in human cancer
460 (Henikoff et al. 2025; Zheng et al. 2025), suggesting a causal role of increased
461 RNAPIIS5P occupancy at the histone genes cancer development and aging tissues that
462 exhibit stem cell over-proliferation.

463 Materials and Methods

464 Fly Husbandry

465 The *esgGal4/CyO; UAS-GFP/TM6B* strain was a gift from Bruce Edgar. All flies used for
466 chromatin profiling in this study were of the w^{1118} genotype and were maintained at 25˚C.

Downloaded from genome.cshlp.org on June 25, 2026 . Published by Cold Spring Harbor Laboratory Press

467 Virgin females were collected and were kept in uncrowded conditions of 15 or less flies
468 per vial, being flipped every other day to maintain adequate food supply.

469 **Antibodies**

470 Primary antibodies: Anti-H3K27me3: Cell Signaling Technologies cat. no. 9733, lot 19;
471 Anti-RNAPIIS5P: Cell Signaling Technologies cat. no. 13523, lot 3; Anti-Pc: a gift from
472 Judith Kassis; Anti-IgG: Abcam cat. no. ab46540; Anti-GFP: Thermo Fisher Scientific cat.
473 no. 3E6. Secondary antibodies: Guinea pig α-rabbit antibody Antibodies online cat. no.
474 ABIN101961, lot 46671; Anti-mouse-FITC: Jackson Immuno Research cat. no. 115-095-
475 166; Anti-rabbit-Texas Red: Jackson Immuno Research cat. 111-585-144.

476 **Imaging Immunostained guts**

477 Guts from one-day old or forty days old adult females of genotype *esgGal4/CyO; UAS-*
478 *GFP/TM6B* were dissected, incubated in Accutase (Stem Cell Technologies cat. 07922)
479 for 10mins, and fixed in 4% formaldehyde/PBS with 0.1% Triton X-100 (PBST) for 10
480 minutes, incubated in 0.3% sodium deoxycholate/PBST 2× for 10 minutes twice (Lim and
481 Fuller 2012), and then incubated with primary antibodies (1:100 dilution) in Goat Serum
482 (Fisher Scientific cat. 16-210-072) in PBS buffer at 4°C overnight and then with
483 fluorescently-labeled secondary antibodies (1:200 dilution, Jackson ImmunoResearch)
484 for two hours at room temperature. Guts were stained with 0.5 µg/mL DAPI/PBS and
485 mounted in 80% glycerol on slides and imaged by epifluorescence on Leica Stellaris8
486 Confocal at the Fred Hutch Cellular Imaging Shared Resource and processed using Fiji
487 software (Schindelin et al. 2012).

488 **Smurf Assay**

Downloaded from genome.cshlp.org on June 25, 2026 . Published by Cold Spring Harbor Laboratory Press

489 The Smurf assay was conducted as previously described in (Martins et al. 2018). Smurf
490 food was prepared by adding non-absorbable blue dye (FD&C Blue No. 1, Sigma-Aldrich,
491 catalog number: 861146) to standard fly food at a final concentration of 2.5% (w/v). Virgin
492 female flies were collected and maintained at a density of 20 flies per vial. Flies were
493 monitored daily for signs of "Smurfness" (blue dye outside of the digestive tract indicating
494 intestinal barrier failure) and survival. Flies were flipped daily on to fresh Smurf food.

495 **SciCUT&Tag library preparation**

496 40 midguts per age were dissected in 1× PBS, working 10 at a time and moving into a
497 1.5mL tube containing 1× PBS on ice during processing. Once 40 midguts of one age
498 were dissected, they were moved to a petri dish in a drop of 1× PBS on ice and chopped
499 with a razor. Chopped up tissue was moved to a tube containing 160 μL of 2mg/mL
500 collagenase (Millipore Sigma cat # C9407) with 50 mM HEPES and 360 μM $CaCl_2$ for 1
501 hour at room temperature with gentle vortexing every 15 minutes. We then added 10uL
502 of 0.5M EDTA to inhibit the collagenase and spun down the samples at 600×g for 3mins
503 and removed the supernatant. The remainder of the procedure was performed following
504 the sciCUT&Tag protocol described in (Janssens et al. 2024). Two iCell8 chips (TaKaRa,
505 cat. no. 640019) were ran and sequenced on Illumina NextSeq 2000 using a the P1-100
506 flow cell at Fred Hutchinson Cancer Center Genomics Shared Resource.

507 **Bulk Chromatin Profiling**

508 We dissected guts from female flies of 1, 15, and 40 days old in 1× PBS, working 10 at a
509 time and moving into a 1.5mL tube containing 1× PBS on ice during processing. Four
510 replicates per age per epitope of profiling reactions were performed, with 5 guts per

Downloaded from genome.cshlp.org on June 25, 2026 . Published by Cold Spring Harbor Laboratory Press

511 reaction. Each sample was digested in 50 µL of 2mg/mL collagenase (Millipore Sigma cat
512 # C9407) containing 50 mM HEPES and 360 µM $CaCl_2$ 1hr at room temperature with
513 gentle vortexing every 15 minutes. After dissociation, 5uL of Concanavalin-A-conjugated
514 magnetic beads (ConA beads, Bangs Laboratories cat #BP531) were added and allowed
515 to bind at room temperature for 10 minutes. Buffer exchange was performed on a
516 magnetic stand (MACSiMAG Seperator cat #130-092-168). Bead-bound cells were
517 incubated with primary antibody in Wash buffer (20 mM HEPES pH 7.5, 150 mM NaCl,
518 0.5 mM spermidine, 0.05% Triton X-100 and Roche EDTA-free protease inhibitor)
519 overnight at 4°C, incubated with secondary antibody in Wash buffer for 1 hour at room
520 temperature, and then incubated with protein-A-Tn5 loaded with adapters (Epicypher cat
521 #15-1117) in 300-Wash buffer (20 mM HEPES pH 7.5, 300 mM NaCl, 0.5 mM spermidine,
522 0.05% Triton X-100 with Roche cOmplete protease inhibitor) for 1 hour. After one wash
523 with 300Wash+ buffer, samples were incubated in CUTAC-DMF Tagmentation buffer (10
524 mM TAPS, 5 mM $MgCl_2$, 20% DMF, 0.05% Triton X-100) for 30 minutes at 37 °C. After
525 tagmentation, samples were washed with TAPS wash buffer (10 mM TAPS, 0.2 mM
526 EDTA). Fragment release was performed in 5 µl 1% SDS supplemented with 1:10
527 Thermolabile Proteinase K (New England Biolabs cat. no. P8111S) at 37 °C for 1 hour
528 followed by 58˚C for 1 hour SDS was quenched by addition of 15 µl 6% Triton X-100 and
529 PCR was performed by addition of 2 µl each barcoded 10mM i5 and i7 primer solutions
530 and 25 µl NEBNext 2× PCR Master mix (New England Biolabs cat. no. ME541L). Libraries
531 were prepared as described (Kaya-Okur et al. 2019; Henikoff et al. 2020) with 14 cycles
532 of PCR with 10 second combined annealing and extension for enrichment of short DNA
533 fragments. Libraries were pooled by volume by epitope and were sequenced in PE50

Downloaded from genome.cshlp.org on June 25, 2026 . Published by Cold Spring Harbor Laboratory Press

534 mode on the Illumina NovaSeq X platform at the Fred Hutchinson Cancer Center
535 Genomics Shared Resource.

536 **Statistics and computational analyses**

537 **Single-cell sequencing analysis**

538 Demultiplexing was performed using the sciCTextract custom software
539 (https://github.com/mfitzgib/sciCTextract) (Janssens et al. 2024). Adapter sequences
540 were cut using cutadapt 2.9 (Martin 2011) with parameters: -j 8 -m 20 -a
541 CTGTCTCTTATACACATCT -A CTGTCTCTTATACACATCT -Z. Sequences were aligned
542 using Bowtie 2 (Langmead and Salzberg 2012) version 2.4.2 to dm6 with parameters: –
543 very-sensitive-local –soft-clipped-unmapped-tlen –no-mixed –no-discordant –dovetail –
544 phred33 -I 10 -X 1000. SAM file created by Bowtie 2 was converted to a BAM file and run
545 ‘bedtools bamtobed -bedpe’ (Quinlan 2014) on the resulting BAM file. For input into the
546 single-cell analysis software ArchR (Granja et al. 2021), we extracted columns 1, 2, 6 and
547 7 of the BED files, which correspond to the chr, start, end and the rewrote the headers to
548 include the barcode. Then the BED files were further processed by reformatting the fourth
549 column to include just the barcode sequence and removing duplicate reads with the same
550 Chromosome, start, stop, and barcode (Janssens et al. 2024). We chose to use the
551 ‘peakmatrix’ option in ArchR to generate the LSI, so to call peaks we merged BAM files
552 from the two iCell8 wafers for each age and used the pseudo-bulk as input into SEACR
553 using the stringent parameter and a cutoff of FDR < 0.01 (Meers et al. 2019)
554 (Supplemental Table S2). Peaks for each age were merged using ‘bedtools merge’. We
555 then made the following cutoffs of our data in ArchR: keeping cells with at least 100

Downloaded from genome.cshlp.org on June 25, 2026 . Published by Cold Spring Harbor Laboratory Press

556 fragments/cell, keeping cells with only a FRIP of 0.7 and greater, and removing cells with
557 a fraction of reads that fell into the blacklist (Amemiya et al. 2019) that was greater than
558 0.2 (Supplemental Tables S3-S5). 100 fragments per cell represents a sequencing depth
559 of 0.000056X coverage per cell for the Drosophila genome, which is greater than what
560 has been reported previously for single-cell CUT&Tag (Wu et al. 2021). We then removed
561 doublets using the ArchR addDoubletScores and filterDoublets functions (Granja et al.
562 2021). For graph-based clustering of sciCUT&Tag data, we used the approach
563 implemented in Seurat (Butler et al. 2018), and then compared common metrics across
564 clusters, including information content (reads/cell) and gene coverage. To annotate cell
565 types using H3K27me3, we calculated chromatin silencing scores as previously reported
566 (Wu et al. 2021). CSS are gene-level, distance-weighted aggregation of single-cell
567 H3K27me3 signal using the ArchR gene activity/score model, which converts fragment
568 counts in tiles around each gene into a depth-normalized score. For H3K27me3, high
569 coverage indicates a 'repressed' status, whereas low coverage indicates 'unrepressed'.

570 Once we had annotated the three cell types (ISCs and EBs were too similar separate into
571 distinct clusters), we exported the barcodes from ArchR and using grep commands,
572 pulled out the fragment information for each cell of each cell type for each age. We then
573 created count tables from the cell-type-specific fragment files using 'bedtools intersect -c'
574 against genes within SEACR peaks (Supplemental Tables S7-S10). Count tables were
575 uploaded to the Degust server (https://degust.erc.monash.edu/) for differential analysis
576 (Supplemental Tables S11-S14). Normalized counts from the count tables were used to
577 generate heatmaps using *ggplot2* (Wickham 2016) in R (R Core Team 2025) for
578 visualization. GO analysis was performed using clusterProfiler (Yu et al. 2012) and

Downloaded from genome.cshlp.org on June 25, 2026 . Published by Cold Spring Harbor Laboratory Press

579 visualized using *ggplot2* (Wickham 2016) in R (R Core Team 2025) (Supplemental Tables
580 S15, S16). BED files from each iCell8 chip were merged and created into normalized
581 count bigwigs by BEDTools (v2.30) (Quinlan 2014) genomecov command with scale
582 (size_of_reference_sequence/total_counts). Normalized count bigwigs are the fraction of
583 counts at each base pair scaled by the size of the reference sequence so that if the counts
584 were uniformly distributed across the genome there would be one at each position. Tracks
585 were uploaded to UCSC Genome Browser and then downloaded as PDF files. For
586 analysis of enhancer regions, a list of curated enhancers from *Drosophila* (Zabidi et al.
587 2015) was downloaded and then filtered for enhancers that fell within our list of
588 H3K27me3 peaks using ‘bedtools intersect’ (Quinlan 2014). We then created count tables
589 for enhancers within peaks from the cell-type-specific fragment files using ‘bedtools
590 intersect -c’. Count tables were uploaded to the Degust server
591 (https://degust.erc.monash.edu/) for differential analysis (Supplemental Tables S17,
592 S18). Differentially enriched enhancers were then used for motif searching using FIMO
593 (Grant et al. 2011) and a list of known transcription factor motifs from JASPAR insect
594 database (Rauluseviciute et al. 2024). Heatmaps and dot plots were generated in R (R
595 Core Team 2025) using *ggplot2* (Wickham 2016).

596 **Bulk sequencing analysis**

597 Adapters were clipped using cutadapt 4.1 with the following parameters: -j 8 --nextseq-
598 trim 20 -m 20 -a AGATCGGAAGAGCACACGTCTGAACTCCAGTCA -A
599 AGATCGGAAGAGCGTCGTGTAGGGAAAGAGTGT -Z. Paired-end reads were mapped
600 to a repeat masked release r6.30 of the *D. melanogaster* genome obtained from UCSC
601 (http://hgdownload.cse.ucsc.edu/goldenPath/dm6/bigZips/dm6.fa.masked.gz) using

Downloaded from genome.cshlp.org on June 25, 2026 . Published by Cold Spring Harbor Laboratory Press

602 Bowtie 2 using the following parameters: --very-sensitive-local --soft-clipped-unmapped-
603 tlen --dovetail --no-mixed --no-discordant -q --phred33 -I 10 -X 1000.

604 Properly paired reads were extracted from the alignments by SAMtools (v1.14) (Danecek
605 et al. 2021) bamtobed command into mapped fragment BED files. Replicate BED files
606 were merged and created into normalized count bigwigs by BEDTools (v2.30) genomecov
607 command with scale (size_of_reference_sequence/total_counts). Normalized count
608 bigwigs are the fraction of counts at each base pair scaled by the size of the reference
609 sequence so that if the counts were uniformly distributed across the genome there would
610 be one at each position. Comparisons between Pc and IgG signal for promoters in
611 Supplmental Table S25 was performed using normalized count bigwigs using UCSC tools
612 BigWigAverageOverBed (Kent et al. 2010).

613 Count tables were generated using BED files using 'bedtools intersect -c' against
614 promoter list of the dm6 genome version 31 downloaded from FlyBase. Normalized
615 counts from the count tables were used to generate heatmaps using *ggplot2* in R (R Core
616 Team 2025) for visualization (Supplemental Tables S22, S23) (Wickham 2016).
617 Aggregate plots with heatmaps were generated using deepTools2 (Ramirez et al. 2016).

618 **Data access:**

619 All raw and processed sequencing data generated in this study have been deposited in
620 the NCBI Gene Expression Omnibus (GEO; https://www.ncbi.nlm.nih.gov/geo/) database
621 undeaccession code GSE291173. sciCTextract custom software for demultiplexing
622 sciCUT&Tag can be found on GitHub (https://github.com/mfitzgib/sciCTextract).

623 **Competing interest statement:**

Downloaded from genome.cshlp.org on June 25, 2026 . Published by Cold Spring Harbor Laboratory Press

624 K.A. and S.H. have filed patent applications on related work. The other authors declare
625 no competing interests.

626 **Acknowledgements**

627 We thank C. Codomo, J. Henikoff, and M. Fitzgibbons for technical assistance, the Fred
628 Hutchinson Cancer Center Genomics Shared Resource for sequencing and data
629 processing, and at Fred Hutchinson Cancer Center Cellular Imaging Shared Resource
630 for assistance with microscopy and image analysis and members of the Henikoff lab for
631 helpful discussions. This work was supported by the Howard Hughes Medical Institute (to
632 S.H.) and NIH Ruth L. Kirschstein National Research Service Award 1F32GM153148-01
633 (to S.M.L.). *Author contributions:* S.M.L., K.A, and S.H. designed the study. S.M.L.
634 performed the experiments and analyzed the data. K.A. and S.H. supervised the study.
635 S.M.L wrote the original draft and all authors reviewed and approved the manuscript.

636 **References**
637

638 Aguilera J, Duan J, Cortez K, Lee RS, Aragon A, Ray M, Larschan E. 2025. The CLAMP
639 GA-binding transcription factor regulates heat stress-induced transcriptional
640 repression by associating with 3D chromatin loops. *bioRxiv*
641 doi:10.1101/2023.10.08.561401.
642 Akkouche A, Kneuss E, Bornelov S, Renaud Y, Eastwood EL, van Lopik J, Gueguen N,
643 Jiang M, Creixell P, Maupetit-Mehouas S et al. 2025. Binding of heterochromatin
644 protein Rhino to a subset of piRNA clusters depends on a combination of two
645 histone marks. *Nat Struct Mol Biol* **32**: 1517-1527.
646 Altman DG, Bland JM. 1983. Measurement in Medicine: The Analysis of Method
647 Comparison Studies. *The Statistician* **32**: 307-317.
648 Amemiya HM, Kundaje A, Boyle AP. 2019. The ENCODE Blacklist: Identification of
649 Problematic Regions of the Genome. *Sci Rep* **9**: 9354.
650 Biteau B, Hochmuth CE, Jasper H. 2008. JNK activity in somatic stem cells causes loss
651 of tissue homeostasis in the aging Drosophila gut. *Cell Stem Cell* **3**: 442-455.
652 Biteau B, Jasper H. 2014. Slit/Robo signaling regulates cell fate decisions in the intestinal
653 stem cell lineage of Drosophila. *Cell Rep* **7**: 1867-1875.
654 Blackledge NP, Klose RJ. 2021. The molecular principles of gene regulation by Polycomb
655 repressive complexes. *Nat Rev Mol Cell Biol* **22**: 815-833.

Downloaded from genome.cshlp.org on June 25, 2026 . Published by Cold Spring Harbor Laboratory Press

656 Boyer LA, Plath K, Zeitlinger J, Brambrink T, Medeiros LA, Lee TI, Levine SS, Wernig M,
657 Tajonar A, Ray MK et al. 2006. Polycomb complexes repress developmental
658 regulators in murine embryonic stem cells. *Nature* **441**: 349-353.
659 Brown JL, Sun MA, Kassis JA. 2018. Global changes of H3K27me3 domains and
660 Polycomb group protein distribution in the absence of recruiters Spps or Pho. *Proc*
661 *Natl Acad Sci U S A* **115**: E1839-E1848.
662 Buchon N, Osman D, David FP, Fang HY, Boquete JP, Deplancke B, Lemaitre B. 2013.
663 Morphological and molecular characterization of adult midgut
664 compartmentalization in Drosophila. *Cell Rep* **3**: 1725-1738.
665 Butler A, Hoffman P, Smibert P, Papalexi E, Satija R. 2018. Integrating single-cell
666 transcriptomic data across different conditions, technologies, and species. *Nat*
667 *Biotechnol* **36**: 411-420.
668 Cao R, Wang L, Wang H, Xia L, Erdjument-Bromage H, Tempst P, Jones RS, Zhang Y.
669 2002. Role of histone H3 lysine 27 methylation in Polycomb-group silencing.
670 *Science* **298**: 1039-1043.
671 Capo F, Wilson A, Di Cara F. 2019. The Intestine of Drosophila melanogaster: An
672 Emerging Versatile Model System to Study Intestinal Epithelial Homeostasis and
673 Host-Microbial Interactions in Humans. *Microorganisms* **7**.
674 Clark RI, Salazar A, Yamada R, Fitz-Gibbon S, Morselli M, Alcaraz J, Rana A, Rera M,
675 Pellegrini M, Ja WW et al. 2015. Distinct Shifts in Microbiota Composition during
676 Drosophila Aging Impair Intestinal Function and Drive Mortality. *Cell Rep* **12**: 1656-
677 1667.
678 Danecek P, Bonfield JK, Liddle J, Marshall J, Ohan V, Pollard MO, Whitwham A, Keane
679 T, McCarthy SA, Davies RM et al. 2021. Twelve years of SAMtools and BCFtools.
680 *Gigascience* **10**: giab008.
681 Denecke S, Fusetto R, Batterham P. 2017. Describing the role of Drosophila
682 melanogaster ABC transporters in insecticide biology using CRISPR-Cas9
683 knockouts. *Insect Biochem Mol Biol* **91**: 1-9.
684 Denell RE, Frederick RD. 1983. Homoeosis in Drosophila: a description of the Polycomb
685 lethal syndrome. *Dev Biol* **97**: 34-47.
686 Dutta D, Dobson AJ, Houtz PL, Glasser C, Revah J, Korzelius J, Patel PH, Edgar BA,
687 Buchon N. 2015. Regional Cell-Specific Transcriptome Mapping Reveals
688 Regulatory Complexity in the Adult Drosophila Midgut. *Cell Rep* **12**: 346-358.
689 El Mai M, Bird M, Allouche A, Targen S, Serifoglu N, Lopes-Bastos B, Guigonis JM, Kang
690 D, Pourcher T, Yue JX et al. 2023. Gut-specific telomerase expression counteracts
691 systemic aging in telomerase-deficient zebrafish. *Nat Aging* **3**: 567-584.
692 Emerson FJ, Lee SS. 2023. Chromatin: the old and young of it. *Front Mol Biosci* **10**:
693 1270285.
694 Feser J, Truong D, Das C, Carson JJ, Kieft J, Harkness T, Tyler JK. 2010. Elevated
695 histone expression promotes life span extension. *Mol Cell* **39**: 724-735.
696 Granja JM, Corces MR, Pierce SE, Bagdatli ST, Choudhry H, Chang HY, Greenleaf WJ.
697 2021. ArchR is a scalable software package for integrative single-cell chromatin
698 accessibility analysis. *Nat Genet* **53**: 403-411.
699 Grant CE, Bailey TL, Noble WS. 2011. FIMO: scanning for occurrences of a given motif.
700 *Bioinformatics* **27**: 1017-1018.

Downloaded from genome.cshlp.org on June 25, 2026 . Published by Cold Spring Harbor Laboratory Press

701 Havas A, Yin S, Adams PD. 2022. The role of aging in cancer. *Molecular oncology* **16**:
702 3213-3219.
703 Henikoff S, Henikoff JG, Kaya-Okur HS, Ahmad K. 2020. Efficient chromatin accessibility
704 mapping in situ by nucleosome-tethered tagmentation. *Elife* **9**: e63274.
705 Henikoff S, Zheng Y, Paranal RM, Xu Y, Greene JE, Henikoff JG, Russell ZR, Szulzewsky
706 F, Thirimanne HN, Kugel S et al. 2025. RNA polymerase II at histone genes
707 predicts outcome in human cancer. *Science* **387**: 737-743.
708 Huang SK, Whitney PH, Dutta S, Shvartsman SY, Rushlow CA. 2021. Spatial
709 organization of transcribing loci during early genome activation in Drosophila. *Curr*
710 *Biol* **31**: 5102-5110 e5105.
711 Hung RJ, Hu Y, Kirchner R, Liu Y, Xu C, Comjean A, Tattikota SG, Li F, Song W, Ho Sui
712 S et al. 2020. A cell atlas of the adult Drosophila midgut. *Proc Natl Acad Sci U S A*
713 **117**: 1514-1523.
714 Janssens DH, Greene JE, Wu SJ, Codomo CA, Minot SS, Furlan SN, Ahmad K, Henikoff
715 S. 2024. Scalable single-cell profiling of chromatin modifications with sciCUT&Tag.
716 *Nat Protoc* **19**: 83-112.
717 Janssens DH, Otto DJ, Meers MP, Setty M, Ahmad K, Henikoff S. 2022. CUT&Tag2for1:
718 a modified method for simultaneous profiling of the accessible and silenced
719 regulome in single cells. *Genome Biol* **23**: 81.
720 Jenkins NL, McColl G, Lithgow GJ. 2004. Fitness cost of extended lifespan
721 inCaenorhabditis elegans. *Proceedings of the Royal Society of London Series B:*
722 *Biological Sciences* **271**: 2523-2526.
723 Jiang H, Patel PH, Kohlmaier A, Grenley MO, McEwen DG, Edgar BA. 2009.
724 Cytokine/Jak/Stat signaling mediates regeneration and homeostasis in the
725 Drosophila midgut. *Cell* **137**: 1343-1355.
726 Josserand M, Rubanova N, Stefanutti M, Roumeliotis S, Espenel M, Marshall OJ, Servant
727 N, Gervais L, Bardin AJ. 2023. Chromatin state transitions in the Drosophila
728 intestinal lineage identify principles of cell-type specification. *Dev Cell* **58**: 3048-
729 3063 e3046.
730 Kassis JA, Kennison JA, Tamkun JW. 2017. Polycomb and Trithorax Group Genes in
731 Drosophila. *Genetics* **206**: 1699-1725.
732 Katheder NS, Browder KC, Chang D, De Maziere A, Kujala P, van Dijk S, Klumperman J,
733 Lu TC, Li H, Lai Z et al. 2023. Nicotinic acetylcholine receptor signaling maintains
734 epithelial barrier integrity. *Elife* **12**: e86381.
735 Kaya-Okur HS, Janssens DH, Henikoff JG, Ahmad K, Henikoff S. 2020. Efficient low-cost
736 chromatin profiling with CUT&Tag. *Nat Protoc* **15**: 3264-3283.
737 Kaya-Okur HS, Wu SJ, Codomo CA, Pledger ES, Bryson TD, Henikoff JG, Ahmad K,
738 Henikoff S. 2019. CUT&Tag for efficient epigenomic profiling of small samples and
739 single cells. *Nat Commun* **10**: 1930.
740 Kent WJ, Zweig AS, Barber G, Hinrichs AS, Karolchik D. 2010. BigWig and BigBed:
741 enabling browsing of large distributed datasets. *Bioinformatics* **26**: 2204-2207.
742 Kim YK, Cho B, Cook DP, Trcka D, Wrana JL, Ramalho-Santos M. 2023. Absolute scaling
743 of single-cell transcriptomes identifies pervasive hypertranscription in adult stem
744 and progenitor cells. *Cell Rep* **42**: 111978.
745 Kim YK, Collignon E, Martin SB, Ramalho-Santos M. 2024. Hypertranscription: the
746 invisible hand in stem cell biology. *Trends Genet* **40**: 1032-1046.

Downloaded from genome.cshlp.org on June 25, 2026 . Published by Cold Spring Harbor Laboratory Press

747 Konno K, Mitsuhashi W. 2019. The peritrophic membrane as a target of proteins that play
748 important roles in plant defense and microbial attack. *J Insect Physiol* **117**: 103912.
749 Krause SA, Overend G, Dow JAT, Leader DP. 2022. FlyAtlas 2 in 2022: enhancements to
750 the Drosophila melanogaster expression atlas. *Nucleic Acids Res* **50**: D1010-
751 D1015.
752 Langmead B, Salzberg SL. 2012. Fast gapped-read alignment with Bowtie 2. *Nat*
753 *Methods* **9**: 357-359.
754 Leader DP, Krause SA, Pandit A, Davies SA, Dow JAT. 2018. FlyAtlas 2: a new version
755 of the Drosophila melanogaster expression atlas with RNA-Seq, miRNA-Seq and
756 sex-specific data. *Nucleic Acids Res* **46**: D809-D815.
757 Lehane MJ. 1997. Peritrophic matrix structure and function. *Annu Rev Entomol* **42**: 525-
758 550.
759 Li H, Qi Y, Jasper H. 2016. Preventing Age-Related Decline of Gut Compartmentalization
760 Limits Microbiota Dysbiosis and Extends Lifespan. *Cell Host Microbe* **19**: 240-253.
761 Liang J, Balachandra S, Ngo S, O'Brien LE. 2017. Feedback regulation of steady-state
762 epithelial turnover and organ size. *Nature* **548**: 588-591.
763 Lim JG, Fuller MT. 2012. Somatic cell lineage is required for differentiation and not
764 maintenance of germline stem cells in Drosophila testes. *Proc Natl Acad Sci U S*
765 *A* **109**: 18477-18481.
766 Loubiere V, Delest A, Thomas A, Bonev B, Schuettengruber B, Sati S, Martinez AM,
767 Cavalli G. 2016. Coordinate redeployment of PRC1 proteins suppresses tumor
768 formation during Drosophila development. *Nat Genet* **48**: 1436-1442.
769 Ma Z, Wang H, Cai Y, Wang H, Niu K, Wu X, Ma H, Yang Y, Tong W, Liu F et al. 2018.
770 Epigenetic drift of H3K27me3 in aging links glycolysis to healthy longevity in
771 Drosophila. *Elife* **7**: e35368.
772 Mahat DB, Tippens ND, Martin-Rufino JD, Waterton SK, Fu J, Blatt SE, Sharp PA. 2024.
773 Single-cell nascent RNA sequencing unveils coordinated global transcription.
774 *Nature* **631**: 216-223.
775 Martin M. 2011. Cutadapt removes adapter sequences from high-throughput sequencing
776 reads. *EMBnetjournal* **17**: 1138-1143.
777 Martins RR, McCracken AW, Simons MJP, Henriques CM, Rera M. 2018. How to Catch
778 a Smurf? - Ageing and Beyond... In vivo Assessment of Intestinal Permeability in
779 Multiple Model Organisms. *Bio Protoc* **8**.
780 Marzluff WF, Koreski KP. 2017. Birth and Death of Histone mRNAs. *Trends Genet* **33**:
781 745-759.
782 Meers MP, Tenenbaum D, Henikoff S. 2019. Peak calling by Sparse Enrichment Analysis
783 for CUT&RUN chromatin profiling. *Epigenetics Chromatin* **12**: 42.
784 Metchnikoff E, Mitchell P. 1907. *The prolongation of life; optimistic studies*. G.P. Putnam
785 Sons, London.
786 Micchelli CA, Perrimon N. 2006. Evidence that stem cells reside in the adult Drosophila
787 midgut epithelium. *Nature* **439**: 475-479.
788 Niccoli T, Partridge L. 2012. Ageing as a risk factor for disease. *Curr Biol* **22**: R741-752.
789 Ohlstein B, Spradling A. 2006. The adult Drosophila posterior midgut is maintained by
790 pluripotent stem cells. *Nature* **439**: 470-474.

Downloaded from genome.cshlp.org on June 25, 2026 . Published by Cold Spring Harbor Laboratory Press

791 Orsi GA, Kasinathan S, Hughes KT, Saminadin-Peter S, Henikoff S, Ahmad K. 2014.
792 High-resolution mapping defines the cooperative architecture of Polycomb
793 response elements. *Genome Res* **24**: 809-820.
794 Parreno V, Loubiere V, Schuettengruber B, Fritsch L, Rawal CC, Erokhin M, Gyorffy B,
795 Normanno D, Di Stefano M, Moreaux J et al. 2024. Transient loss of Polycomb
796 components induces an epigenetic cancer fate. *Nature* **629**: 688-696.
797 Quinlan AR. 2014. BEDTools: The Swiss-Army Tool for Genome Feature Analysis. *Curr*
798 *Protoc Bioinformatics* **47**: 11 12 11-34.
799 R Core Team. 2025. R: A Language and Environment for Statistical Computing. R
800 Foundation for Statistical Computing, Vienna, Austria.
801 Ramirez F, Ryan DP, Gruning B, Bhardwaj V, Kilpert F, Richter AS, Heyne S, Dundar F,
802 Manke T. 2016. deepTools2: a next generation web server for deep-sequencing
803 data analysis. *Nucleic Acids Res* **44**: W160-165.
804 Rauluseviciute I, Riudavets-Puig R, Blanc-Mathieu R, Castro-Mondragon JA, Ferenc K,
805 Kumar V, Lemma RB, Lucas J, Cheneby J, Baranasic D et al. 2024. JASPAR 2024:
806 20th anniversary of the open-access database of transcription factor binding
807 profiles. *Nucleic Acids Res* **52**: D174-D182.
808 Rera M, Bahadorani S, Cho J, Koehler CL, Ulgherait M, Hur JH, Ansari WS, Lo T, Jr.,
809 Jones DL, Walker DW. 2011. Modulation of longevity and tissue homeostasis by
810 the Drosophila PGC-1 homolog. *Cell Metab* **14**: 623-634.
811 Rera M, Clark RI, Walker DW. 2012. Intestinal barrier dysfunction links metabolic and
812 inflammatory markers of aging to death in Drosophila. *Proc Natl Acad Sci U S A*
813 **109**: 21528-21533.
814 Rodriguez-Fernandez IA, Tauc HM, Jasper H. 2020. Hallmarks of aging Drosophila
815 intestinal stem cells. *Mech Ageing Dev* **190**: 111285.
816 Salazar AM, Aparicio R, Clark RI, Rera M, Walker DW. 2023. Intestinal barrier dysfunction:
817 an evolutionarily conserved hallmark of aging. *Dis Model Mech* **16**: dmm049969.
818 Schaaf CA, Misulovin Z, Gause M, Koenig A, Gohara DW, Watson A, Dorsett D. 2013.
819 Cohesin and polycomb proteins functionally interact to control transcription at
820 silenced and active genes. *PLoS Genet* **9**: e1003560.
821 Schindelin J, Arganda-Carreras I, Frise E, Kaynig V, Longair M, Pietzsch T, Preibisch S,
822 Rueden C, Saalfeld S, Schmid B et al. 2012. Fiji: an open-source platform for
823 biological-image analysis. *Nat Methods* **9**: 676-682.
824 Schwartz YB, Kahn TG, Nix DA, Li XY, Bourgon R, Biggin M, Pirrotta V. 2006. Genome-
825 wide analysis of Polycomb targets in Drosophila melanogaster. *Nat Genet* **38**: 700-
826 705.
827 Siebold AP, Banerjee R, Tie F, Kiss DL, Moskowitz J, Harte PJ. 2010. Polycomb
828 Repressive Complex 2 and Trithorax modulate Drosophila longevity and stress
829 resistance. *Proc Natl Acad Sci U S A* **107**: 169-174.
830 Siudeja K, van den Beek M, Riddiford N, Boumard B, Wurmser A, Stefanutti M, Lameiras
831 S, Bardin AJ. 2021. Unraveling the features of somatic transposition in the
832 Drosophila intestine. *EMBO J* **40**: e106388.
833 Sun D, Luo M, Jeong M, Rodriguez B, Xia Z, Hannah R, Wang H, Le T, Faull KF, Chen R
834 et al. 2014. Epigenomic profiling of young and aged HSCs reveals concerted
835 changes during aging that reinforce self-renewal. *Cell Stem Cell* **14**: 673-688.

Downloaded from genome.cshlp.org on June 25, 2026 . Published by Cold Spring Harbor Laboratory Press

836 Tauc HM, Rodriguez-Fernandez IA, Hackney JA, Pawlak M, Ronnen Oron T, Korzelius J,
837 Moussa HF, Chaudhuri S, Modrusan Z, Edgar BA et al. 2021. Age-related changes
838 in polycomb gene regulation disrupt lineage fidelity in intestinal stem cells. *Elife* **10**:
839 e62250.
840 Wickham H. 2016. ggplot2 : Elegant Graphics for Data Analysis. In *Use R!*,,
841 doi:10.1007/978-3-319-24277-4, pp. 1 online resource (XVI, 260 pages 232
842 illustrations, 140 illustrations in color. Springer International Publishing : Imprint:
843 Springer,, Cham.
844 Williams GC. 1957. Pleiotropy, Natural Selection, and the Evolution of Senescence.
845 *Evolution* **11**: 398-411.
846 Wu SJ, Furlan SN, Mihalas AB, Kaya-Okur HS, Feroze AH, Emerson SN, Zheng Y,
847 Carson K, Cimino PJ, Keene CD et al. 2021. Single-cell CUT&Tag analysis of
848 chromatin modifications in differentiation and tumor progression. *Nat Biotechnol*
849 **39**: 819-824.
850 Yang N, Occean JR, Melters DP, Shi C, Wang L, Stransky S, Doyle ME, Cui CY, Delannoy
851 M, Fan J et al. 2023. A hyper-quiescent chromatin state formed during aging is
852 reversed by regeneration. *Mol Cell* **83**: 1659-1676 e1611.
853 Yu G, Wang LG, Han Y, He QY. 2012. clusterProfiler: an R package for comparing
854 biological themes among gene clusters. *OMICS* **16**: 284-287.
855 Zabidi MA, Arnold CD, Schernhuber K, Pagani M, Rath M, Frank O, Stark A. 2015.
856 Enhancer-core-promoter specificity separates developmental and housekeeping
857 gene regulation. *Nature* **518**: 556-559.
858 Zhang C, Ding Y, Zhou M, Tang Y, Chen R, Chen Y, Wen Y, Wang S. 2023. RNAi-mediated
859 CHS-2 silencing affects the synthesis of chitin and the formation of the peritrophic
860 membrane in the midgut of Aedes albopictus larvae. *Parasit Vectors* **16**: 259.
861 Zheng Y, Ahmad K, Henikoff S. 2025. Total whole-arm chromosome losses predict
862 malignancy in human cancer. *Proc Natl Acad Sci U S A* **122**: e2505385122.
863 Zhu H, Ludington WB, Spradling AC. 2024. Cellular and molecular organization of the
864 Drosophila foregut. *Proc Natl Acad Sci U S A* **121**: e2318760121.
865 Zhuang X, Wang Q, Joost S, Ferrena A, Humphreys DT, Li Z, Blum M, Krause K, Ding S,
866 Landais Y et al. 2025. Ageing limits stemness and tumorigenesis by
867 reprogramming iron homeostasis. *Nature* **637**: 184-194.

868

869

870

871

872

873

874 **Figure Legends**

875 **Figure 1. Repressed landscapes for cell types in the Drosophila gut.**

Downloaded from genome.cshlp.org on June 25, 2026 . Published by Cold Spring Harbor Laboratory Press

876 *(A)* Immunofluorescence image of the gut in a young *esgGal4/CyO; UAS-GFP/TM6B*
877 female**.** GFP (green) marks stem cells and enteroblasts, red anti-H3K27me3, DAPI in
878 grey. Pink arrowhead points to ISC/EBs, blue arrowhead points to enterocytes, and yellow
879 arrowhead points to enteroendocrine cells. Enterocytes are the large DAPI stained nuclei
880 (blue arrow). Enteroendocrine cells are identified by their small nucleus size in relation to
881 the larger enterocytes and low GFP signal (yellow arrows). (*B*) UMAP of H3K27me3
882 signal in gut cells from 1-, 15-, and 40-day-old females. Clusters are assigned cell types
883 by low CSS score at marker genes. (*C*) Violin plots of the distribution of fragments per
884 cell for 1-day-old cell types. (*D*) Log_2 transformed counts per kilobase per million (CPKM)
885 normalized and *Z*-score normalized heatmaps from differential analysis of H3K27me3
886 over genes between 1day old cell types. (*E-H*) UCSC Genome Browser tracks of
887 repressed domains in the three cell types in young guts. (*E*) The *ANTP-C* domain is
888 shared between all three cell types. (*F*) A domain encompassing the piRNA cluster *42AB*
889 is present only in ISC/EBs, (*G*) a domain encompassing the *lncRNA:CR32773* gene is
890 present only in enteroendocrine cells, and (*H*) a domain encompassing the *how* gene is
891 present only in enterocytes.

892

893 **Figure 2. Changes in repressed landscapes in gut cells with age.**

894 (*A-C*) UMAPs of cell types from guts of different ages. Enteroendocrine cells and
895 ISC/EBs of different ages are mixed within cell type clusters, but enterocytes form three
896 separate clusters. (*D-F*) *Z*-score normalized heatmaps from differential analysis of
897 H3K27me3 signal over genes between young and old cells. The first column of each
898 heatmap is the log_2 transformed counts per kilobase per million (CPKM) for 1-day old

Downloaded from genome.cshlp.org on June 25, 2026 . Published by Cold Spring Harbor Laboratory Press

899 cells for each cell type. (*D*) ISC/EBs have an almost equal number of genes that lose (39
900 genes) and gain (36 genes) H3K27me3 signal with age. (*E*) Enteroendocrine cells show
901 a greater number of losses of H3K27me3 signal (237 genes) compared to a gain in
902 H3K27me3 signal (40 genes) with age. (*E*) Enterocytes have the greatest number of
903 genes that show a change in H3K27me3 signal with age (1588 genes) with an age-
904 related gain in H3K27me3 signal in 878 genes. It should be noted that genes that gain
905 H3K27me3 signal are weak domains in young cells and genes that show a loss of
906 H3K27me3 signal are strong domains in young cells. (*G,H*) Genome browser tracks of
907 genes that are differentially methylated in enterocytes, showing a loss (*G*) and gain (*H*)
908 in H3K27me3 signal with age.

909

910 **Figure 3. Repression of barrier genes in aged enterocytes.**

911 (*A*) Results of a Smurf assay in which flies are fed food containing a non-absorbable blue
912 dye. Fly on the left is 1 day old and has the blue dye is restricted to the digestive tract.
913 Fly on the right is 40 days old and the blue dye can be seen throughout the entire body.
914 (*B*) Top four GO terms on genes that gain H3K27me3 signal in aged enterocytes from
915 differential analysis. (*C-D*) UCSC Genome Browser tracks of chitin synthesis (*C*) and
916 chitinase (*D*) genes that form new H3K27me3 domains in aged enterocytes. (*E*) Row *z*-
917 score normalized heatmap of RNAPIIS5P counts over chitin synthesis gene promoters.
918 The first column of each heatmap is the $\log_2$ transformed counts for 1-day old tissue for
919 each promoter. Row *z*-scoring is used to present directionality of the change in signal
920 with age. (*F-G*) UCSC Genome Browser track of Polycomb in 1-dayold guts at the

Downloaded from genome.cshlp.org on June 25, 2026 . Published by Cold Spring Harbor Laboratory Press

921 promoter of the *Chs2* gene (*F*) and at *Cht9* (*G*). (*H*) Heatmap of log_2 transformed counts
922 for Polycomb binding at each chitin synthesis gene promoter.

923

924 **Figure 4. Stem cells display overproliferation and derepression of lineage-**
925 **specifying genes and JAK/STAT ligands.**

926 (*A*) Row *z*-score normalized heatmap of H3K27me3 counts of ISC/EBs for
927 enteroendocrine genes defined in Fig. 1D. The first column is the log_2 transformed counts
928 per kilobase per million (CPKM) for 1-day old tissue for each gene. (*B*)
929 Immunofluorescence image of the gut in a young (1 day old) and old (40 days old)
930 *esgGal4/CyO; UAS-GFP/TM6B* female**.** GFP (green) marks stem cells and enteroblasts
931 and DAPI in grey. (*C*) Pie charts of the proportion of each cell type per age. Significance
932 was assessed by Monte Carlo permutation test (10,000 permutations). Observed
933 enrichment was greater than expected by chance ($p < 0.0001$).(*D*) Row *z*-score
934 normalized heatmap of H3K27me3 counts over the *Unpaired* domain, which
935 encompasses three genes encoding JAK/STAT ligands**.** The first column is the log_2
936 transformed counts for 1-day old tissue for each promoter. ISC/EBs have the lowest
937 H3K27me3 level of the three cell types in 1-day old tissue and lose H3K27me3 signal
938 with age, indicating derepression. Row *z*-scoring is used to present directionality of the
939 change in signal with age. (*E*) Row *z*-score normalized heatmap of RNAPIIS5P counts
940 over promoters of the *Upd1*, *Upd2*, and *Upd3* genes. The first column is the log_2
941 transformed counts for 1-day old tissue for each promoter. *Upd2* and *Upd3* gain
942 RNAPIIS5P signal in aged tissues which is consistent with previous reports of these
943 ligands. Row *z*-scoring is used to present directionality of the change in signal with age.

Downloaded from genome.cshlp.org on June 25, 2026 . Published by Cold Spring Harbor Laboratory Press

944 **Figure 5. S-phase histone genes are upregulated with global downregulation in**
945 **aged guts.**

946 (*A*) RNAPIIS5P counts for the absolute difference (40 days old– 15 days old) counts
947 versus average count ($\log_{10}$(40 days old + 15 days old)/2) for all promoters in the
948 Drosophila genome. (*B*) UCSC Genome Browser track of RNAPIIS5P at a representative
949 histone gene repeat. Yellow boxes highlight the promoter region of each histone gene.
950 (*C*) Bar charts depicting RNAPIIS5P counts per million (CPM) for each promoter of the
951 histone gene repeat shown in panel (*B*). Significance was assessed Poisson rate test
952 compared to 15 days old samples with asterisks indicating $p < 0.05$ (*), p < 0.01 (**), p <
953 0.001 (***), and p < 0.0001 (****).

954 **Figure 6. Model for cell-type-specific Polycomb remodeling drives gut aging.**

955 **(*A*) Young gut:** The epithelium is composed primarily of enterocytes, with a small
956 population of ISC/EBs. In enterocytes, Polycomb (Pc) binds chitin-related promoters (e.g.,
957 *Chs2*, *Cht* cluster) but H3K27me3 levels remain low, allowing robust RNAPII occupancy
958 and continuous peritrophic-matrix production. Stem cells proliferate at homeostatic rates
959 and show low RNAPII occupancy at S-phase histone loci.

960 **(B) Mid-age gut:** Enterocyte numbers decline while ISC/EBs expand. H3K27me3
961 signal accumulates at Pc-bound chitin genes in enterocytes, partially repressing chitin
962 synthesis. The peritrophic matrix becomes thinned, causing moderate luminal stress and
963 a slight increase in enterocyte turnover. Stem cells respond with increased proliferation
964 but maintain low RNAPII at S-phase histone genes.

965 **(C) Old gut:** Enterocytes are markedly depleted and ISC/EBs predominate. In
966 enterocytes, broad Pc-nucleated H3K27me3 domains entirely silence chitin-related loci,

Downloaded from genome.cshlp.org on June 25, 2026 . Published by Cold Spring Harbor Laboratory Press

967 weakening the peritrophic matrix and exposing the epithelium to high luminal stress,
968 further reducing enterocyte numbers. Barrier failure triggers stem cell hyperproliferation
969 and massive RNAPII accumulation at S-phase histone loci—a histone hypertranscription
970 signature resembling that of aggressive tumors.
971

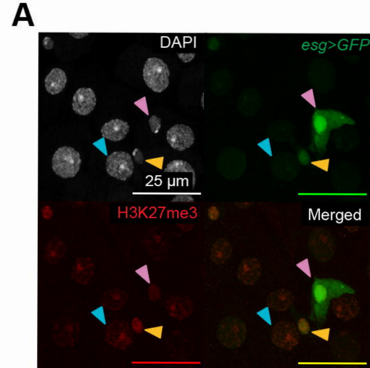
A
DAPI
esg>GFP
25 µm
H3K27me3
Merged

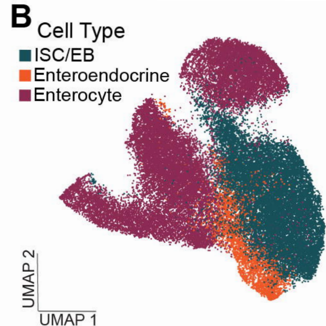
B
Cell Type
ISC/EB
Enteroendocrine
Enterocyte
UMAP 2
UMAP 1

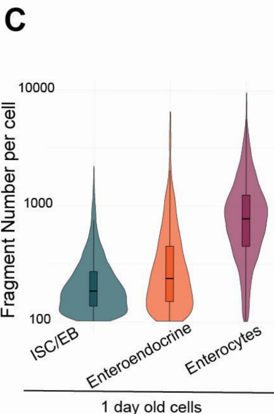
C
Fragment Number per cell
10000
1000
100
ISC/EB
Enteroendocrine
Enterocytes
1 day old cells

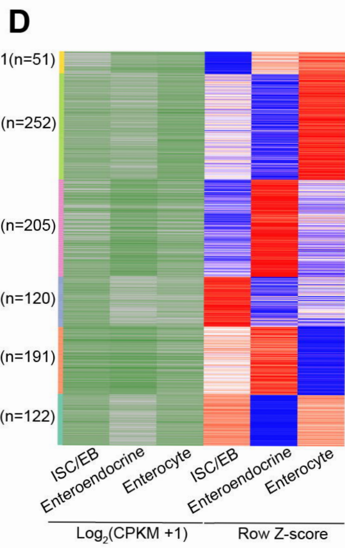
D
Cluster 1(n=51)
Cluster 2 (n=252)
Cluster 3 (n=205)
Cluster 4 (n=120)
Cluster 5 (n=191)
Cluster 6 (n=122)
Log2(CPKM+1)
10.0
7.5
5.0
2.5
0.0
Row Z-Score
1.0
0.5
0.0
−0.5
−1.0
ISC/EB
Enteroendocrine
Enterocyte
ISC/EB
Enteroendocrine
Enterocyte
Log2(CPKM +1)
Row Z-score

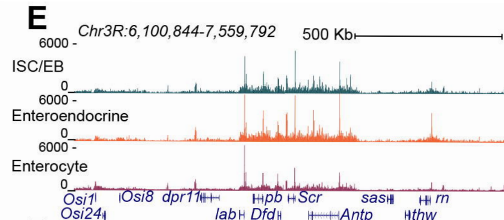
E
Chr3R:6,100,844-7,559,792
500 Kb
6000
ISC/EB
0
6000
Enteroendocrine
0
6000
Enterocyte
0
Osi1
Osi8
dpr11
pb
Scr
sas
rn
Osi24
lab
Dfd
Antp
thw

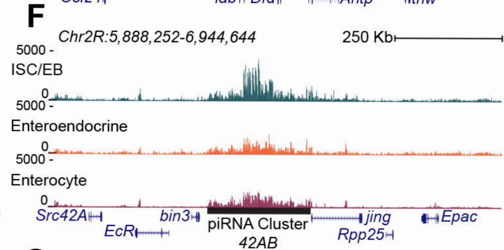
F
Chr2R:5,888,252-6,944,644
250 Kb
5000
ISC/EB
0
5000
Enteroendocrine
0
5000
Enterocyte
0
Src42A
bin3
piRNA Cluster
42AB
jing
Epac
EcR
Rpp25

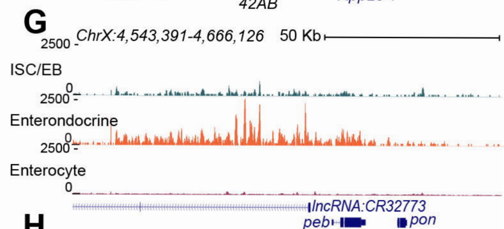
G
ChrX:4,543,391-4,666,126
50 Kb
2500
ISC/EB
0
2500
Enterondocrine
0
2500
Enterocyte
0
lncRNA:CR32773
peb
pon

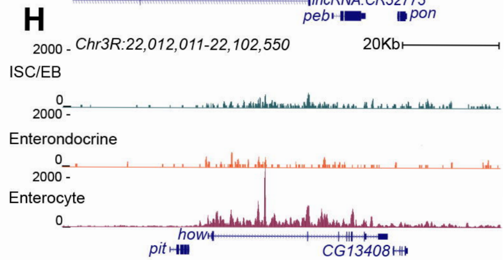
H
Chr3R:22,012,011-22,102,550
20Kb
2000
ISC/EB
0
2000
Enterondocrine
0
2000
Enterocyte
0
how
pit
CG13408

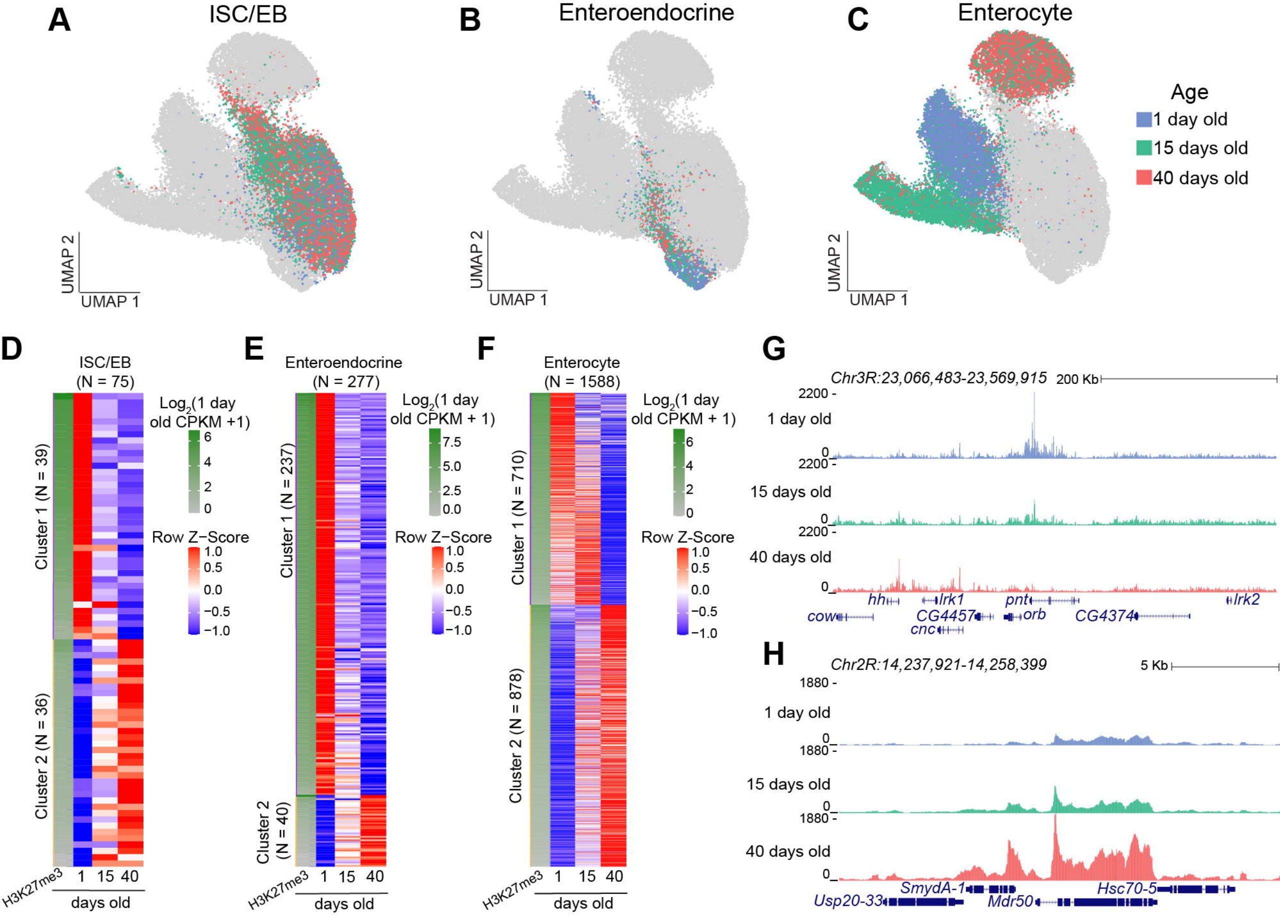

A
ISC/EB
B
Enteroendocrine
C
Enterocyte
Age
1 day old
15 days old
40 days old
UMAP 2
UMAP 1
D
ISC/EB
(N = 75)
Log2(1 day old CPKM +1)
Row Z−Score
Cluster 1 (N = 39)
Cluster 2 (N = 36)
H3K27me3
1
15
40
days old
E
Enteroendocrine
(N = 277)
Cluster 1 (N = 237)
Cluster 2 (N = 40)
F
Enterocyte
(N = 1588)
Cluster 1 (N = 710)
Cluster 2 (N = 878)
G
Chr3R:23,066,483-23,569,915
200 Kb
hh
lrk1
pnt
lrk2
cow
CG4457
orb
CG4374
cnc
H
Chr2R:14,237,921-14,258,399
5 Kb
SmydA-1
Hsc70-5
Usp20-33
Mdr50

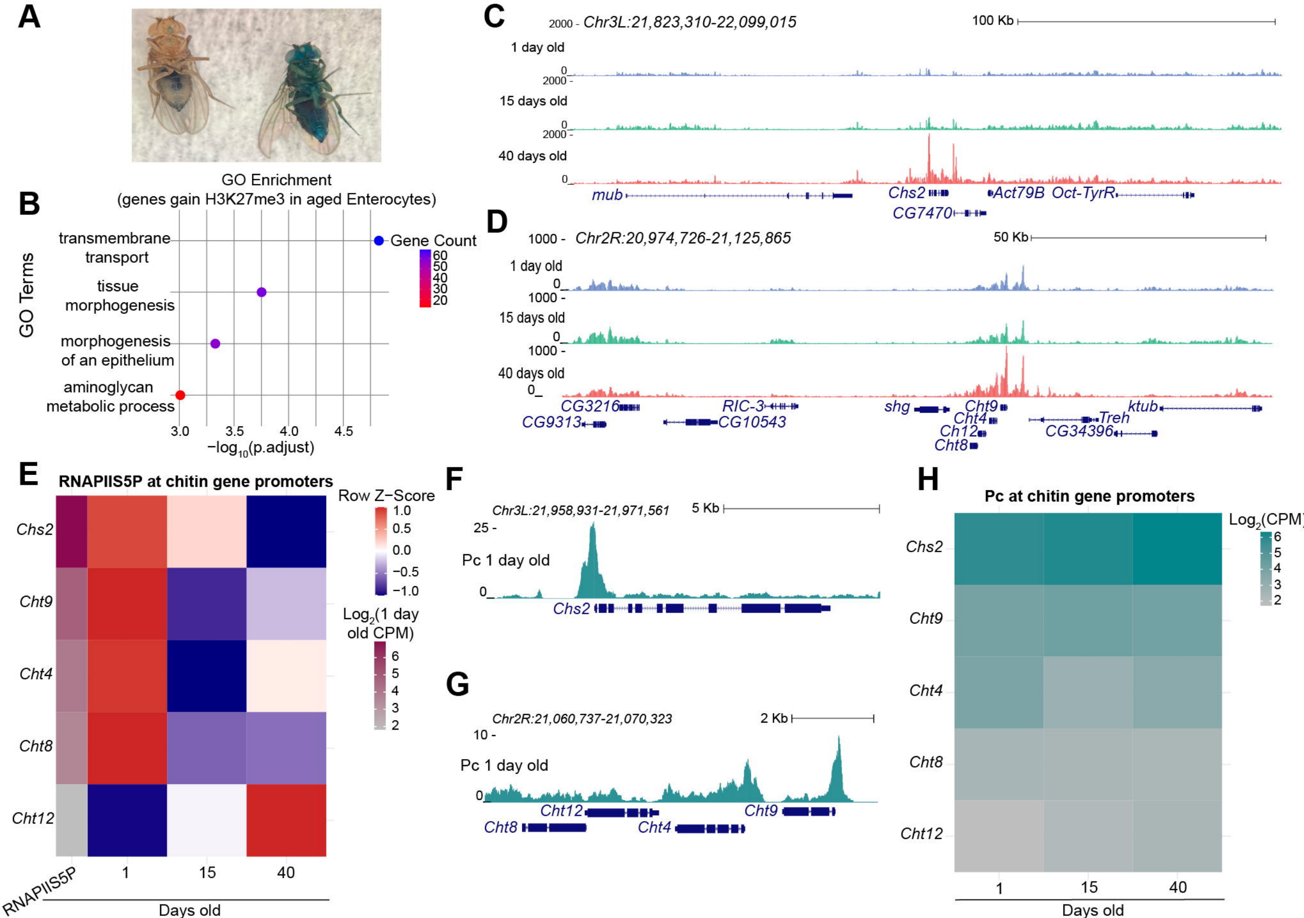
A
B
GO Enrichment
(genes gain H3K27me3 in aged Enterocytes)
GO Terms
transmembrane transport
tissue morphogenesis
morphogenesis of an epithelium
aminoglycan metabolic process
Gene Count
60
50
40
30
20
3.0
3.5
4.0
4.5
−log10(p.adjust)
C
Chr3L:21,823,310-22,099,015
100 Kb
1 day old
15 days old
40 days old
mub
Chs2
Act79B
Oct-TyrR
CG7470
D
Chr2R:20,974,726-21,125,865
50 Kb
1 day old
15 days old
40 days old
CG3216
RIC-3
shg
Cht9
ktub
CG9313
CG10543
Cht4
Treh
Cht12
CG34396
Cht8
E
RNAPIIS5P at chitin gene promoters
Row Z−Score
Log2(1 day old CPM)
Chs2
Cht9
Cht4
Cht8
Cht12
RNAPIIS5P
1
15
40
Days old
F
Chr3L:21,958,931-21,971,561
5 Kb
Pc 1 day old
Chs2
G
Chr2R:21,060,737-21,070,323
2 Kb
Pc 1 day old
Cht12
Cht9
Cht8
Cht4
H
Pc at chitin gene promoters
Log2(CPM)
Chs2
Cht9
Cht4
Cht8
Cht12
1
15
40
Days old

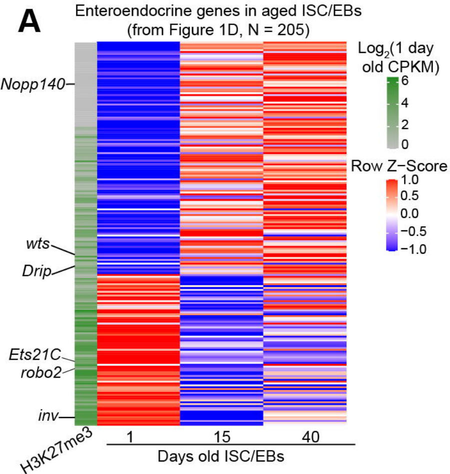
A
Enteroendocrine genes in aged ISC/EBs
(from Figure 1D, N = 205)
Nopp140
wts
Drip
Ets21C
robo2
inv
H3K27me3
1
15
40
Days old ISC/EBs
Log2(1 day old CPKM)
6
4
2
0
Row Z−Score
1.0
0.5
0.0
−0.5
−1.0

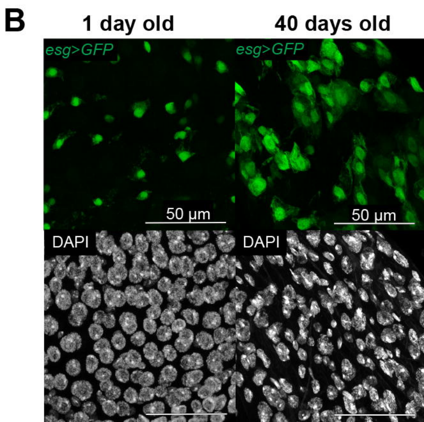
B
1 day old
40 days old
esg>GFP
50 µm
DAPI

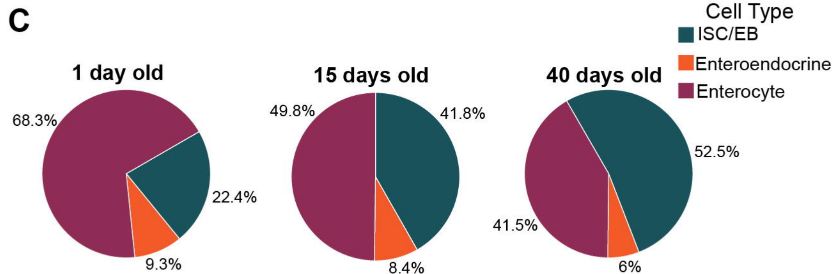
C
1 day old
15 days old
40 days old
68.3%
22.4%
9.3%
49.8%
41.8%
8.4%
52.5%
41.5%
6%
Cell Type
ISC/EB
Enteroendocrine
Enterocyte

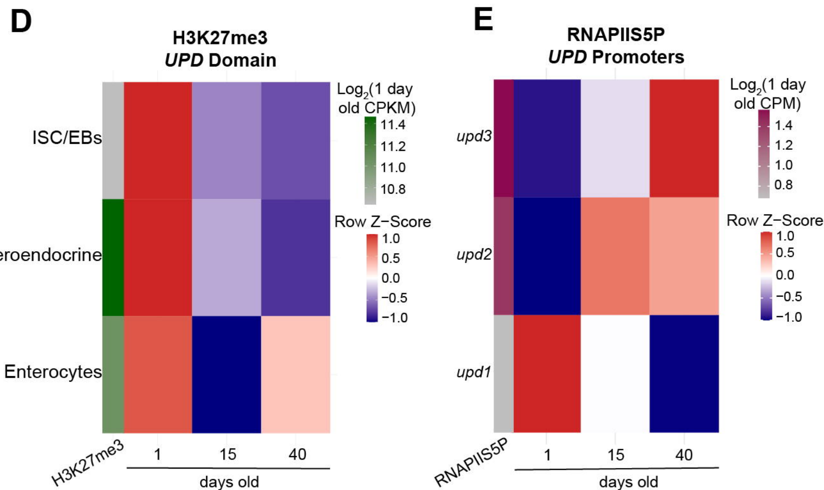
D
H3K27me3
UPD Domain
ISC/EBs
Enteroendocrine
Enterocytes
H3K27me3
1
15
40
days old
Log2(1 day old CPKM)
11.4
11.2
11.0
10.8
Row Z−Score
1.0
0.5
0.0
−0.5
−1.0

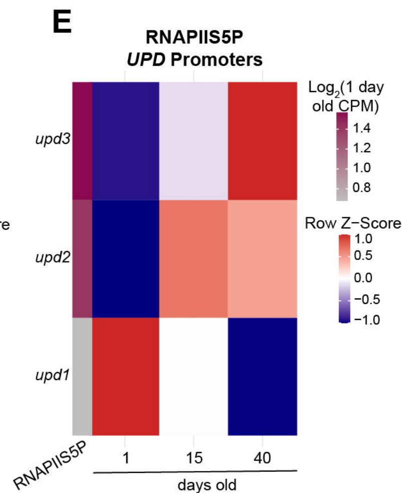
E
RNAPIIS5P
UPD Promoters
upd3
upd2
upd1
RNAPIIS5P
1
15
40
days old
Log2(1 day old CPM)
1.4
1.2
1.0
0.8
Row Z−Score
1.0
0.5
0.0
−0.5
−1.0

A

40 days old vs 15 days old
All promoters (N = 21876)

40 days old vs 15 days old RNAPIIS5P

10000
5000
0

His2A
His2B
His4
His3
His1

Hypertranscription
Hypotranscription

1 10 100 1000 10000

Log_2(RNAPIIS5P)

B

Chr2L:21,455,668-21,460,348

1 Kb

His1 *His2B* *His2A* *His4* *His3*

RNAPIIS5P 1 day old

RNAPIIS5P 15 days old

RNAPIIS5P 40 days old

170 -
0

His1 *His2B* *His2A* *His4* *His3*

C

RNAPIIS5P signal at promoters of histone repeat at *Chr2L:21,455,668-21,460,348*

RNAPIIS5P (CPM)

400
300
200
100
0

****

His1 His2A His2B His3 His4

Age
1
15
40

A

Young

Chitin-related genes

S-phase Histone genes

H1 *H2B* *H2A* *H4* *H3*

B

Mid-age

Chitin-related genes

S-phase Histone genes

H1 *H2B* *H2A* *H4* *H3*

C

Old

Chitin-related genes

S-phase Histone genes

H1 *H2B* *H2A* *H4* *H3*